Intramolecular Magnetic and Electrostatic Interactions in Stepwise Stacked Trinuclear Paramagnetic Metallocenes with the Metal Sequences FeM′Fe and NiM′Ni (M′ = V, Cr, Co, Ni) and CoCrCo†

Hermann Atzkern,[1a] Pierre Bergerat,[1b] Holger Beruda,[1a] Monika Fritz,[1a] Johann Hiermeier,[1a] Peter Hudeczek,[1a] Olivier Kahn,[1b] Frank H. Köhler,*[,1a] Martin Paul,[1a] and Bernd Weber[1a]

Contribution from the Anorganisch-chemisches Institut, Technische Universität München, Lichtenbergstrasse 4, D-85747 Garching, Germany, and Laboratoire de Chimie Inorganique, URA 420, Université de Paris-Sud, F-91405 Orsay, France

Received August 5, 1994[⊗]

Abstract: A building block concept was used for the synthesis of paramagnetic trinuclear metallocenes which are Cp-bridged by two adjacent Me_2Si groups. The series of compounds abbreviated by the metal sequence FeM′Fe contained one central paramagnetic metallocene with M′ = V, Cr, Co, and Ni and two terminal ferrocenes, while three paramagnetic metallocenes were assembled in CoCrCo and the series NiM′Ni with M′ = V, Cr, Co, and Ni. Two paramagnetic centers were present in NiFeNi. The X-ray crystal structure analysis of FeVFe showed a folding of the bridging ligand so that the axes of adjacent metallocenes are inclined by 39.9° and the CH_3 groups are not equivalent (triclinic, space group $P\bar{1}$, a = 10.075(2) Å, b = 10.268(1) Å, c = 9.019(1) Å, α = 96.93(1)°, β = 95.78(1)°, γ = 95.15(1)°, Z = 1). Seven species MM′M were investigated by cyclic voltammetry. They underwent up to five oxidations and two reductions. From the potential splittings Coulomb interactions of 140 and 40 mV were estimated between next-neighbor and terminal metallocenes, respectively. ^1H and ^{13}C NMR studies of the series FeM′Fe established the orbital which is preferred by the unpaired spin and that appreciable spin density is transferred within the bridging ligand from the paramagnetic to the diamagnetic metallocene depending on the folding angle. In the series NiM′Ni and in CoCrCo the spin densities add and subtract depending on the metals. From temperature-dependent ^1H NMR studies of NiVNi and NiNiNi it was concluded that in solution the bending of the molecules decreased with increasing temperature. The ^1H NMR signal widths disclosed magnetic interactions in NiM′Ni. Solid state magnetic measurements on NiVNi, NiCrNi, and NiNiNi showed that the interaction is antiferromagnetic with J = −3.08, −1.95, and −10.5 cm^{-1}, respectively; the Hamiltonian describing the interaction between two local spins is written in the form $-JS_AS_B$. The ground state of these molecules was discussed in terms of a model which relates them to localized trimethylenediyl diradicals.

Introduction

Di- and trinuclear ligand-bridged open-shell metallocenes like **A** and **B** are model compounds for polymers which are expected to exhibit interesting magnetic properties. Among these we have

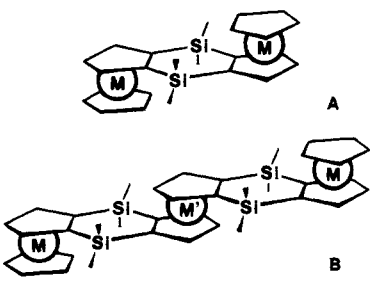

studied molecules of type **B** with a 2-fold concern. Firstly, a general and selective synthesis of sandwich chain fragments that contain alternating paramagnetic centers had to be developed. Secondly, the distribution of the unpaired electron spin density within **B** along with the actual magnetic behavior should provide systematic information on the way to molecular-based magnetic materials, a goal which is presently being pursued very actively by many groups.[2] Among the various contributions which span the full range from organic to inorganic chemistry, there are surprisingly few pure organometallic examples. Some compounds where two or more paramagnetic sandwiches are arranged as next neighbors by a ligand linker to exist,[3] but not all of them are suitable or have been anticipated as building blocks of magnetic materials.

Our guidelines for choosing the bridged Cp (Cp = cyclopentadienyl) ligand **C** (Scheme 1) incorporated in **B** were the following: (i) The Cp−metal bond is rather stable; in particular it is more stable than the arene−metal bond.[4] (ii) Two bridges between the Cps should leave less tortional freedom within **C** than does only one bridge. In fact, we were at first encouraged by the X-ray crystal structure of the dilithium salt of **C** (containing two molecules of TMEDA) which showed a flat bridging ligand.[5] A possible *cis*−*trans* orientation of the metallocene units in **B** should not make matters more complicated. From the results obtained for the dinuclear species **A**[6] it could be expected that when the *cis* arrangement is realized its abundance is small in most cases. So we should be left with

† Dedicated to Professor Hubert Schmidbaur on the occasion of his 60th birthday.

⊗ Abstract published in *Advance ACS Abstracts,* December 15, 1994.

(1) (a) Technische Universität München. (b) Université de Paris-Sud.

(2) Proceedings of the Symposium on the Chemistry and Physics of Molecular Based Magnetic Materials. *Mol. Cryst. Liq. Cryst.* **1993**, *232*, 1−360; *233*, 1−360.

0002-7863/95/1517-0997$09.00/0

Scheme 1

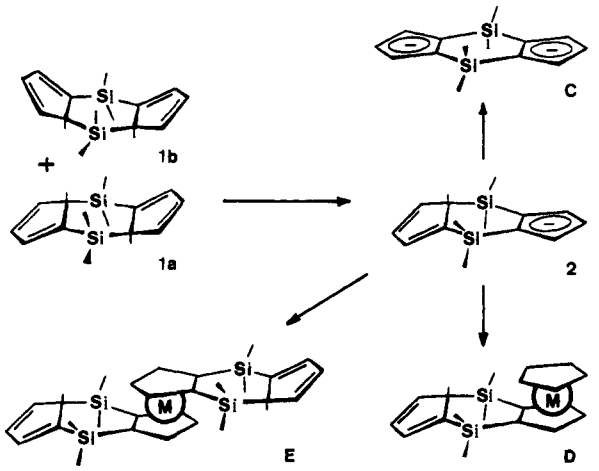

stepwise stacked metallocenes as represented by **B**. This motif is also immanent in most of ref 3, in particular ref 3h. (iii) The hydrocarbon precursor **1a/b**[7] should be readily accessible, a requirement that is now met by synthesizing 60 *g* quantities.[5] (iv) Deprotonation of **1a/b** should proceed cleanly step by step. It turns out that the monoanion **2**[5] is a prerequisite for the selective synthesis of the homo- and heterometallic metallocenes of type **B** via **D**. (v) The building block concept should be applicable not only for the synthesis of the model compounds **B** but also for polymers. It is easy to see that when **2** is transformed to **E** rather than to **D** further deprotonation and reaction with metal dihalides should afford homo- and heterobimetallic metallocene chains with alternating metals. In contrast, **C** should only be useful for the synthesis of homometallic chains.

What magnetic interactions can we expect when linking paramagnetic metallocenes? This question relates our work to concepts that have been developed for organic diradicals.[8] The basis of the relation is that, since all metallocenes have considerable unpaired spin density in their ligand π orbitals, we can tentatively regard the Cp ligand as a radical whose overall spin density is smaller than expected for $S = 1/2$.[9] When we apply this to the bridging ligand in **B**, we can draw **F** where the dots mean that some spin density resides in each of the $2p_z$ orbitals of the five-membered-ring carbon atoms. It is easy to see that the fragment defined by the frame should determine the magnetic interaction between the bridged metallocenes. This fragment is reminescent of the trimethylenediyl-type diradicals (**G**) like cyclobutanediyl (**H**), cyclopentanediyl (**I**), and cyclohexanediyl (**J**). After **I** had been established by Closs,[10] the

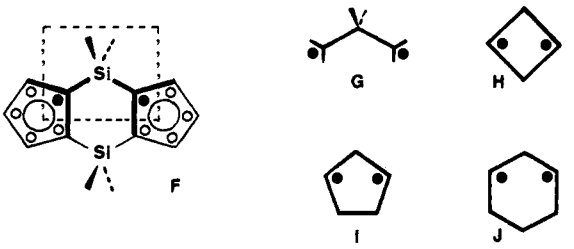

chemistry of cycloalkanediyles was developed systematically by Dougherty.[11] Including theoretical studies[12] it was shown that both ferro- and antiferromagnetic interaction may be found for these diradicals depending on a subtle interplay between (hyperconjugative) through-bond and through-space interaction of the two radical centers. Meanwhile cycloalkanediyls and the like are promising ferromagnetic coupling units for the design of organic magnets.[2,11]

There are some appealing aspects of this approach. Thus, the metallocenes are thermally stable, whereas most alkanediyls must be handled at rather low temperature. In diradicals like **G**–**J** the sign of the spin magnetic moment at the radical centers (the dots) is always positive whereas like and unlike spins may be combined in the stacked metallocenes **B** by choosing appropriate metals. Additional information could be expected for the metallocene derivatives from cyclic voltammetry and NMR spectroscopy—techniques that are usually not applicable for instable organic radicals. In particular, NMR spectroscopy uncovers even small hyperfine interactions in metallocene derivatives, whereas the EPR spectra of diradicals show hyperfine splittings only in a few cases.[13]

(3) (a) Elschenbroich, Ch.; Möckel, R.; Zenneck, U.; Clack, D. W. *Ber. Bunsen-Ges. Phys. Chem.* **1979**, *83*, 1008–1018. (b) Elschenbroich, Ch.; Heck, J. *J. Am. Chem. Soc.* **1979**, *101*, 6773–6776. (c) Elschenbroich, Ch.; Heck, J. *Angew. Chem., Int. Ed. Engl.* **1981**, *20*, 267–269. (d) Köhler, F. H.; Doll, K. H.; Pröβdorf, W.; Müller, J. *Angew. Chem., Int. Ed. Engl.* **1982**, *21*, 151. (e) Lemenowski, D. A.; Urazowski, I. F.; Grishin, Yu. K.; Roznyatovsky, V. A. *J. Organomet. Chem.* **1985**, *290*, 301–305. (f) Bunel, E. E.; Valle, L.; Jones, N. L.; Carroll, P. J.; Gonzales, M.; Munoz, M.; Manriquez, J. M. *Organometallics* **1988**, *7*, 789–791. (g) Heck, J.; Rist, G. *J. Organomet. Chem.* **1988**, *342*, 45–65. (h) Bunel, E. E.; Valle, L.; Jones, N. L.; Carroll, P. J.; Barra, C.; Gonzalez, M.; Munoz, N.; Visconti, G.; Aizman, A.; Manriquez, J. M. *J. Am. Chem. Soc.* **1988**, *110*, 6596–6598. (i) Reiff, W. M.; Manriquez, J. M.; Ward, M. D.; Miller, J. S. *Mol. Cryst. Liq. Cryst.* **1989**, *176*, 423–428. (j) Desbois, M.-H.; Astruc, D.; Guillin, J.; Varret, F.; Trautwein, A. X.; Villeneuve, G. *J. Am. Chem. Soc.* **1989**, *111*, 5800–5809. (k) Bachmann, B.; Hahn, F.; Heck, J.; Wünsch, M. *Organometallics* **1989**, *8*, 2523–2543. (l) Manriquez, J. M.; Ward, M. D.; Calabrese, J. C.; Fagan, P. J.; Epstein, A. J.; Miller, J. S. *Mol. Cryst. Liq. Cryst.* **1989**, *179*, 527–534. (m) Bachmann, B.; Baum, G.; Heck, J.; Massa, W.; Ziegler, B. *Z. Naturforsch. B: Chem. Sci.* **1990**, *45*, 221–238. (n) Bachmann, B.; Heck, J.; Meyer, G.; Pebler, J.; Schleid, T. *Inorg. Chem.* **1992**, *31*, 607–614. (o) Heck, J.; Hermans, P. M. J. A.; Scholten, A. B.; Bosman, W. P. J. H.; Meyer, G.; Staffel, T.; Stürmer, R.; Wünsch, M. *Z. Anorg. Allg. Chem.* **1992**, *611*, 35–42. (p) Hudeczek, P.; Köhler, F. H. *Organometallics* **1992**, *11*, 1773–1775. (q) Stephan, M.; Davis, Jr., J. H.; Meng, X.; Chase, K. J.; Hauss, J.; Zenneck, U.; Pritzkow, H.; Siebert, W.; Grimes, R. N. *J. Am. Chem. Soc.* **1992**, *114*, 5214–5221. (r) Schottenberger, H.; Ingram, G.; Obendorf, D. *J. Organomet. Chem.* **1992**, *426*, 109–119. (s) Delville, M.-H.; Robert, F.; Gouzerh, P.; Linarès, J.; Boukheddaden, K.; Varret, F.; Astruc, D. *J. Organomet. Chem.* **1993**, *451*, C10–C12.

(4) (a) Pilcher, G.; Skinner, H. A. In *The Chemistry of the Metal Carbon Bond*; Hartley, F. R., Patai, S., Eds.; Wiley: New York, 1982; p 43. (b) Dyagileva, L. M.; Tsyganova, E. I.; Aleksandrov, Yu. A. *Russ. Chem. Rev. (Engl. Transl.)* **1988**, *57*, 316–325. (c) Ryan, M. F.; Eyler, J. R.; Richardson, D. E. *J. Am. Chem. Soc.* **1992**, *114*, 8611–8619.

(5) Hiermeier, J.; Köhler, F. H.; Müller, G. *Organometallics* **1991**, *10*, 1787–1793.

(6) Atzkern, H.; Bergerat, P.; Fritz, M.; Hiermeier, J.; Kahn, O.; Kanellakopulos, B.; Köhler, F. H.; Ruhs, M. *Chem. Ber.* **1994**, *127*, 277–286.

(7) (a) Nakadeira, Y.; Sakaba, H.; Sakurai, H. *Chem. Lett.* **1980**, 1071–1074. (b) Barton, T. J.; Burns, G. T.; Arnold, E. V.; Clardy, J. *Tetrahedron Lett.* **1981**, *22*, 7–10. (c) Zemlyanskii, N. N.; Borisova, I. V.; Luzikov, Yu. N.; Ustynyuk, Yu. A.; Kolosova, N. D.; Beletskaya, I. P. *J. Org. Chem. USSR (Engl. Transl.)* **1981**, *17*, 1174–1175. (d) Jones, P. R.; Rozell, Jr., J. M.; Campbell, B. M. *Organometallics* **1985**, *4*, 1321–1324.

(8) (a) Bergmann, R. G. In *Free Radicals*; Kochi, J., Ed.; Academic Press: New York, 1973; Vol. 1, Chapter 5. (b) Borden, W. T., Ed. *Diradicals*; Wiley: New York, 1982.

(9) (a) Köhler, F. H.; Geike, W. *J. Organomet. Chem.* **1987**, *328*, 35–47. (b) Blümel, J.; Hebendanz, N.; Hudeczek, P.; Köhler, F. H.; Strauss, W. *J. Am. Chem. Soc.* **1992**, *114*, 4223–4230. (c) Blümel, J.; Hofmann, P.; Köhler, F. H. *Magn. Reson. Chem.* **1993**, 2–6 (see also earlier papers in the series).

(10) Buchwalter, S. L.; Closs, G. L. *J. Am. Chem. Soc.* **1975**, *97*, 3857–3858; **1979**, *101*, 4688–4694.

(11) Dougherty, D. A. *Acc. Chem. Res.* **1991**, *24*, 88–94.

(12) (a) Conrad, M.; Pitzer, R.; Schaefer, H., III. *J. Am. Chem. Soc.* **1979**, *101*, 2245–2246. (b) Doubleday, C., Jr.; McIver, J. W., Jr.; Page, M. *J. Am. Chem. Soc.* **1982**, *104*, 6533–6542. (c) Goldberg, A. H.; Dougherty, D. A. *J. Am. Chem. Soc.* **1983**, *105*, 284–290. (d) Pranata, J.; Dougherty, D. L. *J. Phys. Org. Chem.* **1989**, *2*, 161–176. (e) Jacobs, S. J.; Shultz, D. A.; Jain, R.; Novak, J.; Dougherty, D. A. *J. Am. Chem. Soc.* **1993**, *115*, 1744–1753.

(13) Jain, R.; Sponsler, M. B.; Coms, F. D.; Dougherty, D. A. *J. Am. Chem. Soc.* **1988**, *110*, 1356–1366 and references cited therein.

Scheme 2[a]

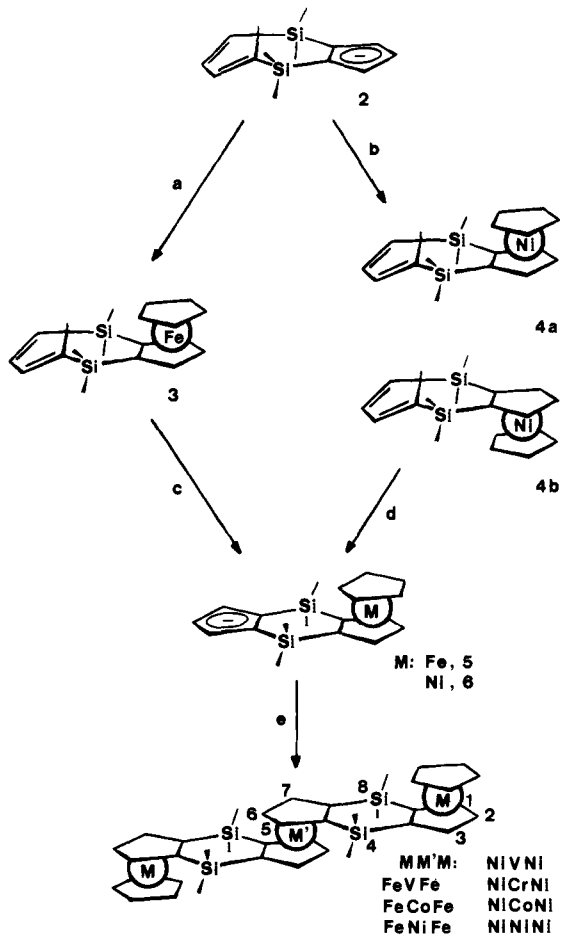

[a] Key: (a) $Cp^-/FeCl_2(THF)_{1.5}$; (b) $Cp^-/NiBr_2(THF)_{1.5}$; (c) nBuLi; (d) $C_5H_{10}NLi$; (e) $VCl_3(THF)_3/Zn$, $CrCl_2(THF)$, $CoCl_2$, $NiBr_2(THF)_{1.5}$, respectively.

In the present work we first investigate how far the unpaired electron spin density in the trimetallic bridged metallocenes **B** is transferred from one moiety to the next. For this purpose we choose the series FeM'Fe[14] where terminal diamagnetic metallocenes monitor the influence of a central paramagnetic metallocene. Next we explore the building block concept for combining two terminal nickelocenes with $S = 1$ or cobaltocenes with $S = 1/2$ with a third paramagnetic metallocene. Emphasis is laid on the concentration of spin on the carbon centers which are equivalent to those in the cycloalkanediyls and on the magnetic interaction between the metallocenes. In addition we investigate inter-metallocene interactions that are disclosed by cyclic voltammetry. A preliminary report on NiCrNi has appeared.[15]

Results

Synthesis. Trinuclear metallocenes having terminal ferrocenes were synthesized by starting with the left part of Scheme 2. The monoanion **2**[5] and an excess of Cp^- were converted to a mixture which contained mainly Cp_2Fe and the ferrocene **3**. Treatment of **3** with nBuLi gave the anion **5**,[16] which reacted with the appropriate halides of vanadium, cobalt, and nickel to afford ocher-yellow FeVFe, orange-brown FeCoFe, and yellow-green FeNiFe in yields of 24–49% after four steps.

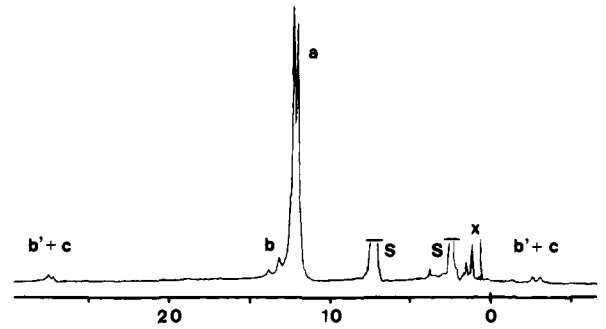

Figure 1. ^1H NMR spectrum of NiNiNi dissolved in toluene-d_8 at 298 K, range of the CH_3 signals: *trans–trans* (a), *cis–trans* (b and b'), *cis–cis* (c). S = solvent, X = impurities, and the scale is in parts per million.

For the series NiM'Ni the diastereomeric mixed-ligand nickelocenes **4a** and **4b** were prepared from **2**, excess Cp^-, and solvated nickel(II) bromide. A compound of type **E** (Scheme 1) may also be formed. It is converted to an insoluble polymer by step e of Scheme 2 and does not influence the result strongly. **4a** and **4b** could be isolated in good yields and fully characterized.[17] However, the isolation proved unnecessary because the anion **6** was insoluble in hexane. Thus, in most cases, after step b of Scheme 2, a slight excess of nickel(II) bromide was removed by extracting all metallocenes with hexane and, after step d, **6** was purified by removing Cp_2Ni again with hexane. It should be noted that unlike **3** the nickelocenes **4a** and **4b** were deprotonated by using lithium piperidide because they are more reactive than ferrocenes. In principle three isomers were expected for the stacked metallocenes MM'M. Thus, the terminal CpM fragments may adopt not only the *trans–trans* orientation relative to the central metal M' (cf. Scheme 2) but also the *cis–trans* and the *cis–cis* orientations depicted below.

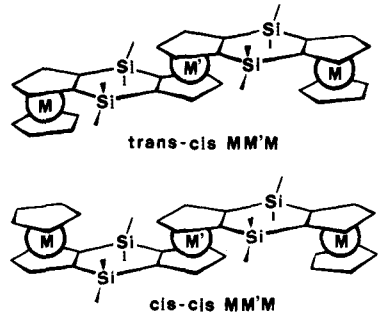

This could be studied conveniently by analyzing the ^1H NMR signals of the $SiCH_3$ groups. Except for NiNiNi we were unable to detect isomers other than *trans–trans* in products that were recrystallized from toluene. In the ^1H NMR spectrum of NiNiNi (Figure 1) the signals of the $SiCH_3$ groups appear in ranges that are well known from the corresponding dinuclear species:[6] 11–14 ppm for *trans* moieties and about 27 and −3 ppm for *cis* moieties. The most intense signals (a) belong to the *trans–trans* isomer. In the low-frequency wings of these signals there are two more (b) which must originate from the *trans* moiety of the *cis–trans* isomer. Corresponding signals are seen in the two *cis* ranges. However, instead of only one signal in each range there are two (b' + c). We conclude that some *cis–cis* isomer was also present.

(14) Throughout this paper we abbreviate the trimetallic molecules **B** as MM'M. See Experimental Section for the systematic names.

(15) Bergerat, P.; Blümel, J.; Fritz, M.; Hiermeier, J.; Hudeczek, P.; Kahn, O.; Köhler, F. H. *Angew. Chem., Int. Ed. Engl.* **1992**, *31*, 1258–1260.

(16) Fritz, M.; Hiermeier, J.; Hertkorn, N.; Köhler, F. H.; Müller, G.; Reber, G.; Steigelmann, O. *Chem. Ber.* **1991**, *124*, 1531–1539.

(17) Fritz, M.; Hiermeier, J.; Köhler, F. H. *Z. Naturforsch. B: Chem. Sci.* **1994**, *49*, 763–769.

Scheme 3[a]

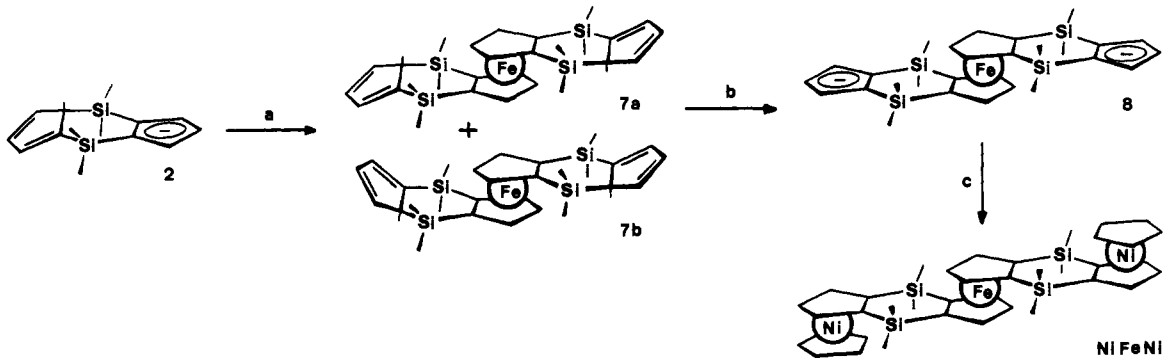

[a] Key: (a) $FeCl_2(THF)_{1.5}$; (b) nBuLi; (c) $Cp^-/NiBr_2(THF)_{1.5}$.

Scheme 4[a]

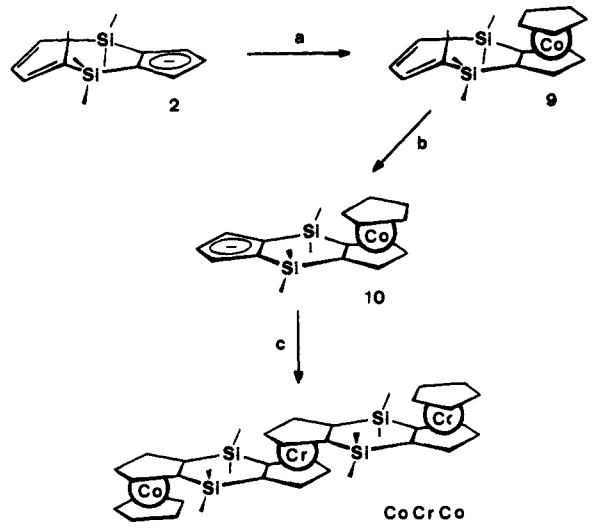

[a] Key: (a) $Cp^-/CoCl_2$; (b) $C_5H_{10}NLi$; (c) $CrCl_2(THF)$.

Trinuclear metallocenes MM'M may be assembled by introducing the bridging ligands not only with the terminal metallocenes (Scheme 2) but also with the central one. The latter approach was realized for NiFeNi (Scheme 3). Thus, the ferrocenes **7a** and **7b** were synthesized from **2** and iron(II) chloride and deprotonated to give **8** as described previously.[16] Addition of an excess of Cp^- and nickel(II) bromide gave olive-green NiFeNi in 51% yield.

Cobaltocene proved to be more difficult to be introduced as a terminal moiety of MM'M because the mixed-ligand cobaltocene anion **10** (Scheme 4) was rather unstable. After the reaction of a mixture of **2** and Cp^- with cobalt(II) chloride and evaporation of the solvents a hexane extract was obtained that had the typical brown color of cobaltocenes. The ^{29}Si NMR spectrum of the crude product showed two signals of approximately equal intensity at −253 and −257 ppm (relative to internal $(Me_3Si)_2O$, half-width 100 Hz, solvent THF, 305 K). This is close to the mean signal shift of −240 ppm per disilated cobaltocene which may be calculated from disilyl-bridged cobaltocenes.[6] It indicates that the mixed-ligand cobaltocene **9** was present in the product which was subsequently subjected to the deprotonation with lithium piperidide. The resulting suspension was separated to yield a brown solid suspected to be the anion **10**. However, after dissolving the solid in THF, the red-brown color soon changed to blue-violet so that we were unable to characterize it by NMR spectroscopy. Nevertheless, the approach could be realized for the pilot compound CoCrCo by rapid reaction of **10** with solvated chromium(II) chloride. Pure CoCrCo proved to be a very air-sensitive green solid which was characterized by mass and NMR spectroscopies. The color of most of the trimetallic species MM'M is mainly derived from the terminal metallocenes. Thus, in the series FeM'Fe yellow to orange predominates while the compounds NiM'Ni are green. CoCrCo is also green whereas its parent compounds Cp_2Co and Cp_2Cr are brown and brick-red, respectively. All compounds are sensitive to air especially in solution; the solubility decreases on passing from THF to toluene and hexane.

In the mass spectra the base peak was associated with the molecular ion. The corresponding peak patterns were in good agreement with the calculated intensities in all cases. Most of the molecules were stable enough to allow the detection of the doubly charged molecular ion. Impurities of the more volatile Cp_2Ni and dinuclear species showed up in the mass spectra of NiVNi and NiCrNi, respectively, although they could not be detected by NMR spectroscopy.

Electrochemistry. The cyclic voltammograms (CVs) were recorded for seven new compounds MM'M under the same conditions: platinum electrodes, solvent propionitrile, conducting salt nBu_4NPF_6, $T \leq -20$ °C. For all electrochemically reversible electron transfers (ETs) the switching potential was separated at least 150 mV from the nearest ET. $Cp_2Co^+PF_6^-$ was added as an internal reference except for FeCoFe and NiCoNi which were measured relative to $Cp_2Fe^{0/+}$ ($E_{1/2}$ = 1345 mV relative to $Cp_2Co^{0/+}$ at −20 °C).

A representative example is FeCrFe whose CV at different temperatures is reproduced in Figure 2. The ETs can be assigned easily by comparison with the half-wave potentials ($E_{1/2}$) of the parent metallocenes.[18] Thus, the ET near 0.3 V belongs to the central chromocene, and those near 1.5 V belong to the ferrocenes. When we compare with the data collected in Table 1, it is clear that successive ETs are well resolved whenever one central and one terminal metallocene are involved. By contrast, the separation of the ETs is much smaller for two terminal metallocenes. In some cases it was necessary to lower the temperature in order to establish the ET splitting (Figure 2); in other cases it could not be resolved at all (Table 1 and Figure 3).

In Figure 2 one of the anodic peaks near 1.5 V appears as a shoulder. For an estimate of the corresponding $E_{1/2}(2)$ value it was assumed that $\Delta E_p(2) \approx \Delta E_P(3)$ where ΔE_p is the difference between the anodic and the cathodic peak potentials (E_a and E_c, respectively). Since $\Delta E_p(3)$ and $\Delta E_p(2)$ are available, we

(18) Connelly, N. G.; Geiger, W. E. *Adv. Organomet. Chem.* **1984**, *23*, 1–93. Strelets, V. V. *Russ. Chem. Rev. (Engl. Transl.)* **1989**, *58*, 297–311. Strelets, V. V. *Coord. Chem. Rev.* **1992**, *114*, 1–60. For $E_{1/2}$ values measured in propionitrile (also used in this work) see ref 6.

(19) Atzkern, H.; Hiermeier, J.; Köhler, F. H.; Steck, A. *J. Organomet. Chem.* **1991**, *408*, 281–296.

(20) Bard, A. J.; Garcia, E.; Kukharenko, S.; Strelets, V. V. *Inorg. Chem.* **1993**, *32*, 3528–3531.

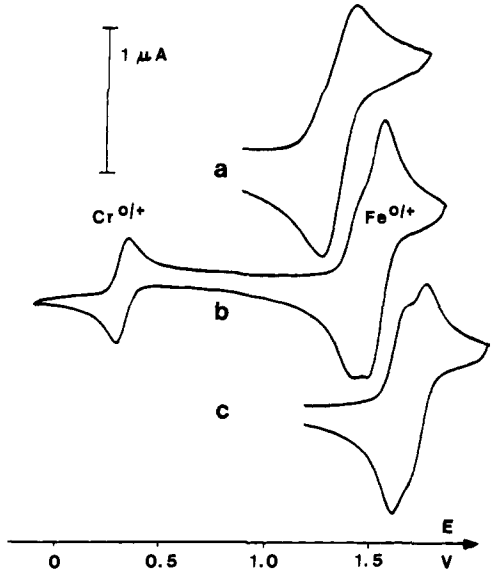

Figure 2. Cyclic voltammograms of the oxidations of FeCrFe in EtCN at 25 °C (a), −20 °C (b), and −40 °C (c). The scan rate is 200 mV cm^{-1}. The potential scale is relative to Cp_2Co/Cp_2Co^+ and only for (b).

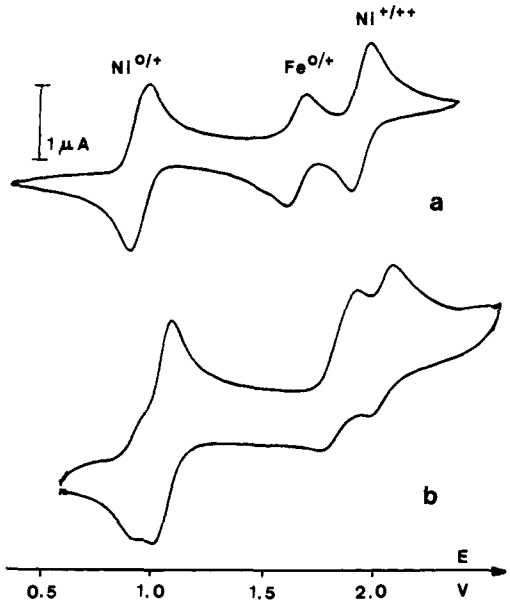

Figure 3. Cyclic voltammograms of the oxidations of NiFeNi (a) and NiCrNi (b) both in EtCN at −20 °C. The scan rate is 200 mV cm^{-1}. The potentials are relative to Cp_2Co/Cp_2Co^+.

get $E_{1/2}(2) \approx E_c(2) + 0.5\ \Delta E_p(3)$. Similar estimates were performed for all overlapping waves. If not stated otherwise, the potential and the reversibility (as derived from the ΔE_p values of the ETs listed in Table 1) do not deviate from what is known for other metallocenes.[18]

For FeVFe two big waves closely following each other were observed in the potential range that is typical for ferrocenes. Another feature appeared at $E_{1/2} \approx 1.1$ V with $\Delta E_p = 160$ mV. This is not far from where the first oxidation of Cp_2V has been located previously.[21a] However, since the electrochemical behavior of Cp_2V is complex[21] and since the intensity of the wave was smaller than expected (i.e., half that of the combined ferrocene waves), we have not analyzed the CV in more detail.

Remarkable differences of the splitting and the reversibility of some ETs were observed in the NiM'Ni series. This is illustrated in Figure 3 where we compare NiCrNi and NiFeNi. For the terminal nickelocenes there are features for the oxidations to both the mono- and the dication leading ultimately to $NiM'Ni^{5+}$ at potentials similar to those of the other nickelocenes.[18] However, the expected splitting for these ETs is only visible for NiCrNi. In addition the terminal nickelocene dications derived from NiFeNi are more stable than those derived from NiCrNi. Thus, the ET of NiFeNi near 1.9 V is quasireversible ($\Delta E_p = 70$ mV, ratio of the anodic and cathodic peak currents 1.2) whereas $NiCrNi^{5+}$ dies away rapidly (EEC mechanism[22]). NiCoNi was found to behave like NiCrNi.

Crystal Structure of FeVFe. As a basis for the understanding of the interaction of the metallocene moieties which is described below, the structure of FeVFe was determined. Crystals were obtained by dissolving the microcrystalline material in a minimum of toluene and cooling the solution to −30 °C. The structure is represented in Figure 4, and important parameters are collected in Table 2.

In the centrosymmetric molecule the metallocene moieties adopt a *trans* arrangement with respect to the Me_2Si bridges. The metal sequence Fe−V−Fe clearly follows from the metal−Cp distances which are significantly longer for the vanadocene moiety (V−D3 1.92 Å) than for the ferrocene moiety (Fe−D1 1.66 Å, Fe−D2 1.63 Å). The values are close to those known for the parent metallocenes.[23] All Cps have mean C−C distances in the usual range (1.40 Å for Cp1 and 1.42 Å for Cp2 and Cp3).

A striking feature is the folding of the bridging ligand backbone. As visualized in Figure 4b the folding is in part due to the silyl substituents bent out of the Cp plane and away from the respective metal (5.7° in the vanadocene, 3.7° in the ferrocene). Since this is opposite to what one would expect from molecular orbital considerations on unsubstituted metal−ring fragments,[24] some constraint must shape the molecule. Actually the CH_3 groups interfere with the adjacent Cp−metal fragments (shortest contacts: C9···V 3.95 Å, C11···V 3.95 Å, C5'···C9 3.84 Å, C10···Fe 4.06 Å, C12···Fe 4.02 Å, C10···C16 3.66 Å) which also causes the fold angle of 149.5° at the Si−Si vector. As a consequence the disilacyclohexadiene part of the bridging ligand adopts the boat conformation characterized by angles of 20.6° and 20.8° between the plane C3a, C4a, C7a, C8a and the planes C3a, Si4, C4a and C7a, Si8, C8a, respectively. The folding leads to a V−Fe distance of 5.98 Å which is 0.35 Å shorter than for an idealized flat structure. Figure 4b also shows a bending of the CH_3 groups away from the adjacent metallocene in such a way that the pairs of plains (C3a, Si4, C4a)/(C11, Si4, C12) and (C7a, Si8, C8a)/(C9, Si8, C10) include angles of 90.3° and 92.2°, respectively. The angle difference (1.9°) demonstrates that the molecule is not located on a crystallographic mirror plane (C_i symmetry).

In the disilacyclohexadiene part of the bridging ligand we have axial and equatorial $Si-CH_3$ bonds. These bonds adopt different orientations relative to the metallocene moieties, which in turn is important for the understanding of the NMR results (vide infra). For instance Figure 4c illustrates the dihedral angles θ between the vanadocene ligand π system (the bond V−C4a serves as a reference for $\theta = 0$) and the bonds Si4−C11 (1.4°) and Si4−C12 (56.3°). For the remaining bond (Si4−C3a) θ is 62.6°. Looking down the bond Si8−C7a (reference bond for $\theta = 0$ is V−C7a), the corresponding θ values are 0.2° (Si8−C9), 59.7° (Si8−C10), and 61.7° (Si8−C8a).

(21) (a) Holloway, J. D. L.; Geiger, W. E. *J. Am. Chem. Soc.* **1979**, *101*, 2038−2044. (b) Mugnier, Y.; Moise, C.; Laviron, E. *Nouv. J. Chim.* **1982**, *6*, 197−200.

(22) Heinze, J. *Angew. Chem., Int. Ed. Engl.* **1984**, *23*, 831−847.

(23) Haaland, A. *Acc. Chem. Res.* **1979**, *12*, 415−422.

(24) Elian, M.; Chen, M. M. L.; Mingos, D. M. P.; Hoffmann, R. *Inorg. Chem.* **1976**, *15*, 1148−1155.

Table 1. Electrochemical Results[a] of the Trinuclear Metallocenes FeM′Fe (M′ = V, Cr, Fe,[b] Co) and NiM′Ni (M′ = Cr,[c] Fe, Co, Ni)

	FeVFe	FeCrFe	FeFeFe[b]	FeCoFe	NiCrNi[c]	NiFeNi	NiCoNi	NiNiNi[l]
$E_{1/2}(1)$[d]	*f*	320 [Cr]	1310 [Fe]	60 [Co]	340 [Cr]	925 [Ni]	70 [Co]	910 [Ni]
$\Delta E_p(1)$		60	70	80	65	70	90	75
$E_{1/2}(2)$	1425 [Fe]	1480 [Fe]	1370 [Fe]	1475 [Fe]	980 [Ni]	925 [Ni]	945 [Ni]	910 [Ni]
$\Delta E_p(2)$	95	85	70	85	80	70	90	75
$\Delta E_{1/2}(2/1)$[e]		1160	*60*	1415	640	*h*	875	*h*
$E_{1/2}(3)$	1505 [V]	1545 [Fe]	1625 [Fe]	1475 [Fe]	1045 [Ni]	1630 [Fe]	1030 [Ni]	1180 [Ni]
$\Delta E_p(3)$	95	85	70	85	80	80	90	75
$\Delta E_{1/2}(3/2)$[e]	*80*	*65*	255	*h*	*65*	705	*85*	270
$E_{1/2}(4)$					1850 [Ni]	1915 [Ni]	1860 [Ni]	
$\Delta E_p(4)$					170	70	160	
$E_{1/2}(5)$					2040 [Ni]	1915 [Ni]	2010[j] [Ni]	
$\Delta E_p(5)$					105	70		
$\Delta E_{1/2}(5/4)$[e]					*109*	*h*		
$E_{1/2}(-1)$		−1160 [Cr]		−860 [Co]	−1140[g,i]	−1140[g] [Ni]	−1240[g,k]	
$\Delta E_p(-1)$		125		133				
$E_{1/2}(-2)$						−1140[g] [Ni]	−1240[g,k]	

[a] In millivolts relative to Cp_2Co/Cp_2Co^+. Temperature −20 °C except for FeVFe (−28 °C), FeFeFe (−25 °C), and FeCoFe (−23 °C), scan rate 200 mV s^{-1}. [b] From ref 19. [c] From ref 15. [d] Successive anodic and cathodic ETs are numbered in parentheses. The assignment of the individual $E_{1/2}$ values to the various metallocene moieties is given in brackets. [e] ET splittings are given in italics when two terminal metallocenes are involved. [f] A feature was observed which is discussed in the text. [g] Broad irreversible ET; the potential of the reduction peak is given. [h] Splitting not resolved. [i] Unresolved reduction of the nickelocene and chromocene moieties.[20] [j] Reverse peak not resolved; the potential of the oxidation peak is given. [k] Unresolved reduction of the nickelocene and cobaltocene moieties.[20] [l] ETs at higher and lower potentials not investigated.

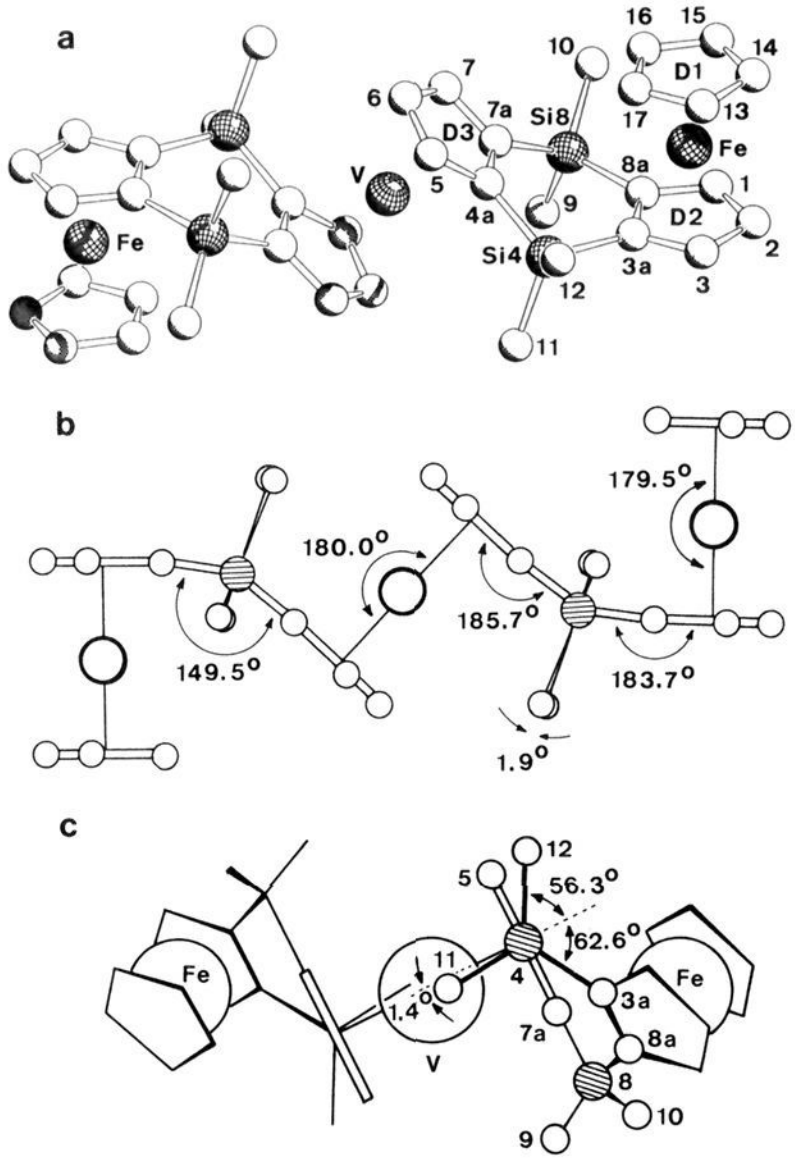

Figure 4. (a) Schakal plot of the molecular geometry of FeVFe (hydrogen atoms omitted). D is the center of the Cp ring. (b) Side view showing the bending angles. (c) View down the bond Si4−C4a showing the dihedral angles θ, i.e., the orientation of the remaining Si−C bonds relative to the vanadocene moiety (cf. also NMR investigation).

NMR Investigation of the Series FeM′Fe. The ^1H and ^{13}C NMR spectra may be decomposed into two sets of signals. One set has strongly shifted and broad signals like those of many other paramagnetic metallocenes, in particular the 1,1′-disilylated derivatives.[9a] The other set has much narrower and less shifted signals which belong to the ferrocene moieties. The shift values are collected in Table 3 where we have also included the unpublished ^{13}C NMR data of FeCrFe.[16] A typical spectrum is shown in Figure 5.

Table 2. Selected Bond Distances (Å) and Angles (deg) for FeVFe with Eds's in Units of the Last Significant Figure in Parentheses

Si4−C4a	1.867(2)	Si8−C3a	1.883(3)
Si4−C7a	1.862(2)	Si8−C8a	1.883(2)
Si4−C11	1.891(1)	Si8−C9	1.873(1)
Si4−C12	1.880(2)	Si8−C10	1.878(2)
Fe−D1[a]	1.66	Fe−D2[a]	1.64
V−D3[a]	1.92	Fe−V	5.97
C3a−Si4−C4a	104.6(1)	C7a−Si8−C8a	104.9(1)
C7a−C4a−Si4	124.5(2)	C4a−C7a−Si8	125.1(2)
C8a−C3a−Si4	125.3(3)	C3a−C8a−Si8	124.4(2)
C3a−Si4−C11	110.2(1)	C7a−Si8−C9	112.6(1)
C3a−Si4−C12	109.8(1)	C7a−Si8−C10	110.3(1)
C4a−Si4−C11	111.8(1)	C8a−Si8−C9	108.9(1)
C4a−Si4−C12	111.2(1)	C8a−Si8−C10	112.6(1)
C11−Si4−C12	109.2(1)	C9−Si8−C10	107.6(1)

[a] Centroid of Cp.

The signal assignment for the paramagnetic metallocene moieties follows from the fact that the electron spin is delocalized directly or indirectly into the Cp π orbitals depicted in Figure 6. As demonstrated previously,[9] the NMR signal sequence of the nuclei of Cp depends on whether spin in π_a or π_s (and their respective sequence of coefficients of the carbon $2p_z$ orbitals) predominates. For instance, in the case of FeCoFe the 1/2/2 pattern of C6, C5/7, and C4a/7a shows the largest signal shift for C6. Consequently, π_s must predominate and the signal shift of C4a/7a must be larger than that of C5/7. For FeVFe only a broad unresolved feature could be detected at −510 ppm for the corresponding carbon atoms, and no reliable result was obtained for FeNiFe although it is known that nickelocene signals should appear near 1500 ppm.[9a,15,25]

Since nothing was known about the spin transfer in FeM′Fe, i.e., from a paramagnetic metallocene M′ to its next neighbor, MO arguments could not be used for the signal assignment of the ferrocene moieties. Instead we took advantage of the unusually narrow ^{13}C NMR signals which displayed the one-bond C−H couplings (Figure 5). By combining this with the

(25) (a) Köhler, F. H.; Doll, K.-H.; Prößdorf, W. *Angew. Chem., Int. Ed. Engl.* **1980**, *19*, 479−480. (b) Köhler, F. H.; Doll, K.-H.; Prößdorf, W. *J. Organomet. Chem.* **1982**, *224*, 341−353. (c) Köhler, F. H.; Doll, K.-H. *Z. Naturforsch. B: Chem. Sci.* **1982**, *37*, 144−150.

Table 3. Paramagnetic ^1H, ^{13}C, and ^{29}Si NMR Signal Shifts[a] at 298 K of the Trinuclear Metallocenes FeM'Fe with M' = V, Cr, Co, and Ni Dissolved in Toluene-d_8

position of nuclei[b]	FeVFe	FeCrFe[c]	FeCoFe	FeNiFe
H (Cp)	1.4	4.9	−1.3	−3.3
H1/3	0.7	−0.8	0.2	0.5
H2	4.8	3.9	0.3	3.2
H5/7	260	256	−33.1	−233
H6	260	212	−55.9	−233
H (CH_3, ax)	23.8	−7.7	−0.1	−1.9
H (CH_3, eq)	4.6	3.4	2.5	6.1
C (Cp)	−11.9	−3.8	13.7	14.7
C1/3	56.9	0.5	0.9	7.6
C2	34.0	25.7	9.9	45.3
C3a/8a	−55.5	19.6	34.7	165.7
C5/7	−795	−548	371	*d*
C6	−495	−136	669	*d*
C4a/7a	−530	−263	584	*d*
C (CH_3, ax)	124	−38.0	75.9	200.1
C (CH_3, eq)	232	−4.3	37.5	128.3
Si4/8	*d*	1174	−201	−867[e]

[a] In parts per million relative to the corresponding signal shifts of the diamagnetic analogue FeFeFe.[19] Since the signals of H1/3 and H5/7, of H2 and H6, and of the two CH_3 groups could not be distinguished, mean values were used. [b] For numbering see Scheme 2. [c] ^1H NMR data taken from ref 16. [d] Not observed. [e] Paramagnetic signal shift at 328 K.

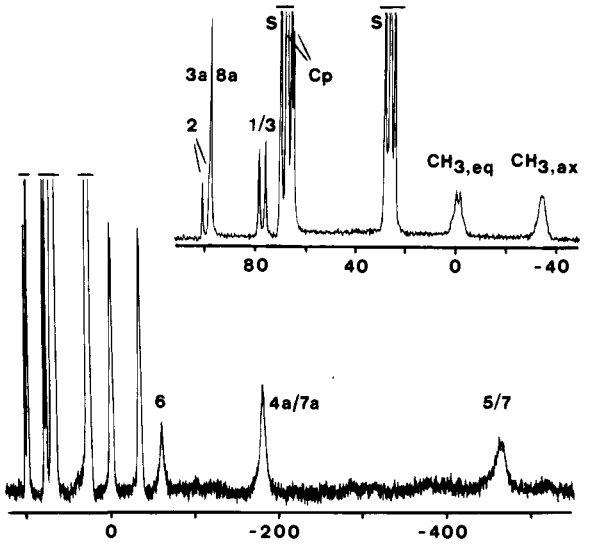

Figure 5. ^{13}C NMR spectrum of FeCrFe dissolved in THF at 303 K. The range −30 to 110 ppm has been expanded in the inset. For numbering see Scheme 2. S = solvent, and the scales are in parts per million.

relative intensities and selective proton decoupling, all ferrocene signals could be identified. The signals of the CH_3 groups were recognized by their quartet structure and/or because they were much broader than the ferrocene signals. This pointed to a predominance of the through-space relaxation.[26] In fact, one of the two ^{13}C NMR signals of the CH_3 groups was always broader than the other one. According to the crystal structure of FeVFe (Figure 4), this must be the axial CH_3 group, which is closer to the paramagnetic center.

The assignment could be confirmed by the ^{13}C NMR signal shifts (Table 3). They are very different because the orientation of the Si−CH_3 bonds relative to the paramagnetic metallocene is different (Figure 4c). As discussed for other metallocenes

(26) (a) Kowalewski, J.; Nordenskiöld, L.; Benetis, N.; Westlund, P. O. *Prog. Nucl. Magn. Reson. Spectrosc.* **1985**, *17*, 141−185. (b) Banci, L.; Bertini, I.; Luchinat, C. *Nuclear and Electron Relaxation*; VCH Publishers: Weinheim, 1991; Chapter 5.

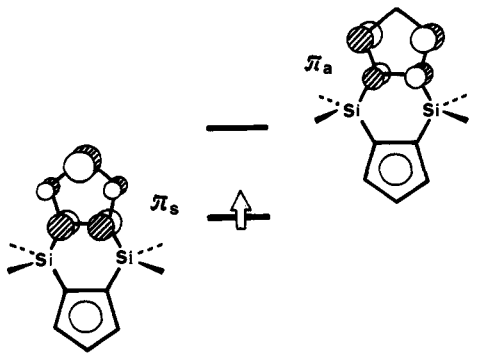

Figure 6. e_1-type π orbitals of one Cp of the bridging ligand, their energy sequence, and the relative spin densities (radii correspond to the coefficients of the carbon $2p_z$ orbitals) when π_a or π_s contribute to the spin-carrying MO. The population preference for FeCoFe is symbolized by the spin arrow.

previously,[9b] the dihedral angle θ between the Cp π orbital and the Si−C bond is related to the contact shift $\delta^{con}(X)$ of any nucleus X by

$$\delta^{con}(X) = \delta_o(X) + B(X)\cos^2\theta \qquad (1)$$

Here $B(X)$ is the constant for the shift caused by the hyperconjugative spin transfer, and $\delta_o(X)$ is the shift caused by other delocalization mechanisms. From eq 1 and the θ values obtained from FeVFe it is evident that throughout the series FeM'Fe the ^{13}C NMR signal of $CH_{3,ax}$ (small θ) must be more shifted than that of $CH_{3,eq}$ (large θ). Depending on the metal, the δ values should be positive (M' = Co, Ni) or negative (M' = V, Cr).[9b] This is in full agreement with our results (Table 3) except for FeVFe. The latter deviates because the spin may be transmitted from vanadium and chromium not only by π polarization but also by σ delocalization as has been outlined previously.[27] This moves the CH_3 signals to high frequency: For M' = Cr the signal shifts have not yet left the negative range; for M' = V they are positive.

The reasoning developed here for assigning the NMR signals is also important for the discussion of the magnetic interaction between neighboring metallocenes of MM'M (cf. below).

NMR Investigation of the Series NiM'Ni and of CoCrCo. All ^1H NMR spectra of NiM'Ni display at least a 5/2/1 signal pattern above 220 ppm, a range which is typical for nickelocenes. When the two signals (area ratio 2/1) of the central metallocene are included, the spectral width may reach almost 500 ppm; an example is NiVNi (Figure 7). The resolution of the signals of the nickelocene and vanadocene moieties is surprisingly good given the fact that usually the splitting should be small.[9c] For NiCrNi the signal of H2 could be observed only below 290 K. The signal assignment follows from the signal areas except for NiNiNi for which other silylated nickelocenes[6,9a] suggest that the shift of the Cp proton signal decreases with increasing number of silyl groups. Hence, the signals of H5/7 and H6 should be less shifted than those of H1/3 and H2, respectively. For the CH_3 groups the signal assignment follows that of the ^{13}C NMR signals discussed below unless the difference of the proton signal shifts is small. Similar arguments apply for the analysis of the spectrum of CoCrCo. The results are listed in Table 4 together with the ^{13}C and ^{29}Si NMR data.

The ^{13}C NMR signals of the central metallocenes of NiM'Ni and CoCrCo appear in ranges similar to those of FeM'Fe, and

(27) Hebendanz, N.; Köhler, F. H.; Müller, G.; Riede, J. *J. Am. Chem. Soc.* **1986**, *108*, 3281−3289.

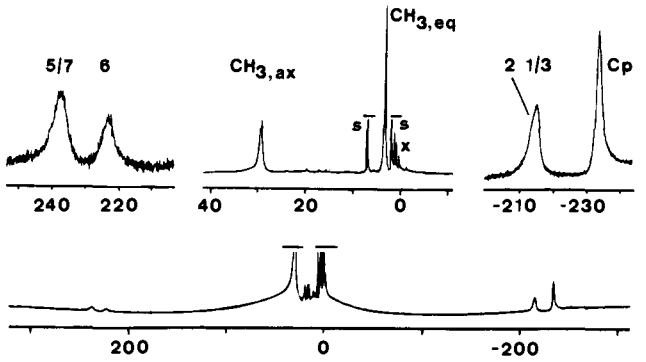

Figure 7. ^{1}H NMR spectrum of NiVNi dissolved in toluene-d_8 at 303 K: bottom, overview; top, relevant ranges expanded. For numbering see Scheme 2. S = solvent, X = impurities, and the scales are in parts per million.

Table 4. Paramagnetic ^{1}H, ^{13}C, and ^{29}Si NMR Signal Shifts[a] at 298 K of the Trinuclear Metallocenes NiM'Ni with M' = V, Cr, Fe, Co, and Ni and CoCrCo Dissolved in Toluene-d_8

position of nuclei[b]	NiVNi	NiCrNi	NiFeNi	NiCoNi	NiNiNi	CoCrCo
H (Cp)	−244	−248	−260	−261	−263	−49.5
H1/3	−225	−230[k]	−234	−237	−242	−37.2
H2	−224	−230[k]	−240	−241	−247	−53.8
H5/7	240	223	−1.1[c]	−30.5	−239	239
H6	224	161	−1.2[c]	−74.2	−243	184
H (CH_3, ax)	29.7[e]	−0.3[e]	6.8	10.1	11.5[e]	2.4[e]
H (CH_3, eq)	2.8[e]	0.1[e]	−2.9	2.8	11.2[e]	−4.2[e]
C (Cp)	*d*	1400	*d*	*d*	*d*	489
C1,2,3,3a,8a	*d*	1420[f]	*d*	*d*	*d*	411[g]
		1440[f]				673[h]
		1460[f]				498[i]
C5/7	−849	−411	29.4	359	*d*	−518
C6	−479	76.8	112.7	873	*d*	−239
C4a/7a	−520	−216.2	133.9	701	*d*	−244
C (CH_3, ax)	268[e]	218.2	242.2	343	*d*	72.8[e]
C (CH_3, eq)	373[e]	−8.0	101.2	251	*d*	−39.2[e]
Si4/8	454	327	−866	−1107	*d*	977

[a] In parts per million. ^{1}H data interpolated from temperature-dependent measurements. [b] For numbering see Scheme 2. [c] In the spectrum the signals coincide accidentally. Different δ values were introduced by the different reference shifts. [d] Not determined. [e] Interchange of signals not excluded. [f] Three shoulders. [g] C1/3. [h] C2. [i] C3a/8a. [k] Separate signals below 280 K with a larger signal shift for H2.

the signal assignment follows the criteria given above. For reasons which have already been mentioned it proved difficult to obtain signals for the terminal nickelocenes. An effort was made for NiCrNi which showed a very broad feature between 1350 and 1600 ppm. The main signal which was attributed to Cp displayed three shoulders at the high-frequency side. Since they could not be assigned, this special range was less informative, and it was not studied for the whole series NiM'Ni.

As outlined in the previous section the ^{13}C NMR signals of the CH_3 groups may be distinguished on the basis of the fact that there must be axial and equatorial CH_3 groups and that the signal of the axial group must be considerably more shifted. However, this is only applicable as long as one of the two paramagnetic metallocenes dominates. When the data of FeM'Fe and NiM'Ni (Tables 3 and 4) are compared, it is clear that all CH_3 groups may be distinguished except for those of NiVNi and CoCrCo.

Magnetic Properties of NiVNi, NiCrNi, and NiNiNi. The magnetic behavior for the three compounds is represented in the form of the χ_mT versus T plot, χ_m being the molar magnetic susceptibility and T the temperature. The curves for NiVNi and NiNiNi are shown in Figure 8. That for NiCrNi has already been interpreted.[15]

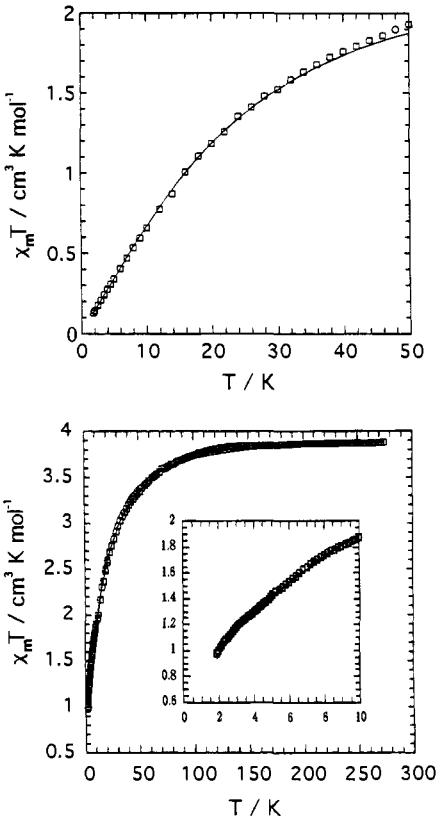

Figure 8. χ_mT vs T plots of NiVNi (bottom) and NiNiNi (top). The best-fit curves were obtained with the parameters given in Table 5.

For NiVNi, χ_mT at room temperature is equal to 3.9 cm^3 K mol^{-1}, which corresponds to what is expected for two $S_{Ni} = 1$ and one $S_V = 3/2$ uncorrelated local spins. As T is lowered χ_mT decreases more and more rapidly and reaches a value of 0.95 cm^3 K mol^{-1} at 1.8 K. For NiNiNi, the magnetic data were only measured below 50 K. χ_mT at 50 K is equal to 1.9 cm^3 K mol^{-1}, which is much lower than expected for three uncorrelated $S_{Ni} = 1$ local spins, and decreases more and more rapidly as T is lowered. χ_mT is equal to 0.12 cm^3 K mol^{-1} at 1.8 K and tends to 0 as T approaches the absolute 0, indicating that the ground state is nonmagnetic.

The spin Hamiltonian used to interpret the magnetic data for both compounds is

$$\mathbf{H} = -J(\mathbf{S}_{Ni1} + \mathbf{S}_{Ni2})\cdot\mathbf{S}_{M'} + \mathbf{S}_{Ni1}\cdot\mathbf{D}_{Ni}\cdot\mathbf{S}_{Ni1} + \mathbf{S}_{Ni2}\cdot\mathbf{D}_{Ni}\cdot\mathbf{S}_{Ni2} + \mathbf{S}_{M'}\cdot\mathbf{D}_{M'}\cdot\mathbf{S}_{M'} + \beta[(\mathbf{S}_{Ni1} + \mathbf{S}_{Ni2})\cdot\mathbf{g}_{Ni} + \mathbf{S}_{M'}\cdot\mathbf{g}_{M'}]\cdot H \quad (2)$$

S_{Ni1} and S_{Ni2} are the local spins for the terminal ions, and $S_{M'}$ is the local spin for the central ion. $\mathbf{D}_{Ni}$ and $\mathbf{D}_{M'}$ are the local anisotropy tensors, and $\mathbf{g}_{Ni}$ and $\mathbf{g}_{M'}$ are Zeeman tensors for the terminal and central ions, respectively. In eq 2 the anisotropic interactions as well as the isotropic interaction between terminal ions are neglected.

From the eigenvalues $E_{i,u}$ of eq 2, when the magnetic H_u field is applied along the u direction, it is possible to determine the molar magnetic susceptibility along this direction as

$$\chi_u = (N\beta/H_u)[\sum_i(-\partial E_{i,u}/\partial H_u)\exp(-E_{i,u}/kT)]/[\sum_i\exp(-E_{i,u}/kT) \quad (3)$$

and then to calculate the average magnetic susceptibility χ_m by averaging over 15 directions of the magnetic field. The local

Table 5. Magnetic Data[a] for NiVNi, NiCrNi, and NiNiNi

	NiVNi	NiCrNi	NiNiNi
g^b	1.99	1.98	1.99
D_{Ni}	24.5	28.7	25.5
$D_{M'}$	*c*	*c*	25.5
J	−3.08	−1.95	−10.5
$R^d \times 10^4$	1.7	3.8	1.5[e]

[a] X_mT in cm³ K mol⁻¹, D and J in cm⁻¹. [b] Assumed to be isotropic and identical for all centers of MM'M. [c] Neglected. [d] Defined as $\Sigma[(\chi_mT)^{cal} - (\chi_mT)^{obs}]^2/\Sigma[(\chi_mT)^{obs}]^2$. [e] After consideration of <1% of a paramagnetic impurity.

anisotropy tensors were assumed to be axial with D_{Ni} (=$3d_{Ni,zz}$/2) and $D_{M',zz}$/2) axial parameters, respectively; the Zeeman tensors were assumed to be isotropic with the same $g_{Ni} = g_{M'} = g$ principal value. The fitting of the experimental data was performed by minimizing R defined as $\Sigma[(\chi_mT)^{obs} - (\chi_mT)^{cal}]^2/[(\chi_mT)^{obs}]^2$.

From the magnetic data concerning both nickelocene and vanadocene, D_{Ni} is known to be large (25−34 cm^{-1} [28]), and D_V is known to be weak and on the order of 2.5 cm^{-1}.[29] Therefore, for NiVNi, D_V was assumed to be negligible with regard to D_{Ni}. For NiNiNi, the local anisotropy tensors were assumed to be equal and coaxial. The parameters deduced from the fitting of the magnetic susceptibility data are gathered in Table 5.

Discussion

The variety of trinuclear metallocenes MM'M demonstrates that the building block approach to bridged metallocenes is widely applicable. In particular side reactions are avoided that occur when the bridging is attempted by substituting the parent paramagnetic metallocenes. When starting with a metallocene which is fused to a cyclopentadiene, the reactions that must be tolerated by the metallocene are deprotonation and the reaction with $M'X_2$. The decomposition may be suppressed by kinetic control (appropriate base and/or temperature). Thus, MM'M with terminal nickelocenes can be obtained in clean reactions, and even the unstable cobaltocene building block **10** (Scheme 4) affords CoCrCo in reasonable yield.

Remarkably, the *trans* linkage between neighboring metallocenes predominates by far, and only for NiNiNi the *cis*−*trans* and *cis*−*cis* isomers could be established. The stereoselectivity is most probably induced by the anionic building blocks **5**, **6**, and **10** because in solid **5** the Cp^- moiety is inclined toward the metallocene[16] while **6** is also folded in solution.[17] Thus, the *trans* face of the Cp moiety is favored by an approaching transition-metal ion.

Interactions of the Charged Trinuclear Metallocenes. In the cyclic voltammogram, molecules having neighboring redox centers display a splitting of the half-wave potentials even if the neighbors are identical. In the latter case the splitting $\Delta E_{1/2}$ surpasses the statistical factor[30] of 36 mV at 25 °C when, after the first electron transfer (ET), the change of the charge at one redox center is transmitted to the second one. For the series MM'M the potential splitting is determined by[30,31] (i) the solvation, (ii) the Coulombic interaction, (iii) the electron delocalization within mixed-valence species, (iv) magnetic interaction (as far as species with two paramagnetic centers are concerned), (v) the substituent effect originating from the silyl bridges, and (vi) the potential shift that occurs upon replacing one metal for another.

Table 6. Metal Influence-Corrected Potential Differences $\Delta E_{1/2}'$ [a] between Redox Waves of MM'M

starting compd	$\Delta E_{1/2}'(1)$[b]	$\Delta E_{1/2}'(2)$[c]	$\Delta E_{1/2}'(1')$[d]	$\Delta E_{1/2}'(2')$[e]
FeFeFe	60	255		
NiNiNi	0	270		
NiFeNi	0	265		
FeCrFe			55	65
NiCrNi			−25	65
FeCoFe			70	0
NiCoNi			−30	85
FeVFe			*f*	80

[a] In millivolts. [b] Potential differences between the electron transfers $MM'M/M^+M'M$ and $M^+M'M/M^+M'M^+$. [c] Potential differences between the electron transfers $M^+M'M/M^+M'M^+$ and $M^+M'M^+/M^+M'^+M^+$. [d] Potential differences between the electron transfers $MM'M/MM'^+M$ and $MM'^+M/M^+M'^+M$. [e] Potential differences between the electron transfers $MM'^+M/M^+M'^+M$ and $M^+M'^+M/M^+M'^+M^+$. [f] The electron transfer $MM'M/MM'^+M$ was not observed.

The latter contribution allows the polarity of the cations derived from MM'M to be adjusted. Thus, either the terminal metallocenes of MM'M (FeFeFe, NiNiNi, and NiFeNi in Table 6) or the central metallocene (all other MM'M) may be oxidized first.

Insight into the interaction of the charged trinuclear metallocenes may be gained when the contributions i−vi to $\Delta E_{1/2}$ are separated. The metal influence (vi) is removed from the experimental data given in Table 1 by subtracting the potential differences found for the parent metallocenes Cp_2M.[6] Here we assume that the differential solvation enthalpy (cf. below) does not change significantly on passing from Cp_2M to MM'M. The so-obtained corrected values $\Delta E_{1/2}'$ are given in Table 6. They show that corresponding ETs are separated by similar $\Delta E_{1/2}'$ values.[32] In particular, this is true for the oxidation of both the trapped mixed-valence ion Ni^+FeNi^+ and the potentially delocalized ions Fe^+FeFe^+ and Ni^+NiNi^+ with $\Delta E_{1/2}'(2)$ near 260 mV. Therefore, the electron delocalization (iii) should not contribute significantly to $\Delta E_{1/2}$. The same is true for the magnetic interaction (iv) because the interaction parameters determined above for MM'M (J < 10 cm^{-1}) are much too small.

As for the Coulombic contribution (ii) two destabilizing interactions (W_1 and W_2) must be considered for the ionic derivatives of MM'M in order to account for the pairs $M^+M'^+$ and $M^+\cdots M^+$, respectively. The influence of the solvation (i) on $\Delta E_{1/2}$ is expressed by the differential solvation free enthalpy[31d] $\Delta\Delta G$. For the oxidations of MM'M we must introduce $\Delta\Delta G_1$ associated with $\Delta E_{1/2}'(1)$ and $\Delta E_{1/2}'(1')$ (cf. Table 6) and $\Delta\Delta G_2$ associated with $\Delta E_{1/2}'(2)$ and $\Delta E_{1/2}'(2')$. Both should be stabilizing because we are dealing with cations in the donor solvent propionitrile. Finally, we must consider the substituent effect E_s (contribution v) whenever in MM'M the number of silyl groups per metallocene changes. This applies to $E_{1/2}(2)$ and $E_{1/2}(1')$ for which E_s has opposite signs. The four corrected

(28) Prins, R.; Van Voorst, J. D. W.; Schinkel, C. J. *Chem. Phys. Lett.* **1967**, *1*, 54−55. Zvarykina, A. V.; Karimov, Yu. S.; Leonova, E. V.; Lyobovskii, R. B. *Fiz. Tverd. Tela* **1970**, *12*, 499−502. Makova, M. K.; Karimov, Yu. S.; Leonova, E. V. *Theor. Exp. Chem. (Engl. Transl.)* **1972**, *8*, 340−343. Baltzer, P.; Furrer, A.; Hulliger, J.; Stebler, A. *Inorg. Chem.* **1988**, *27*, 1543−1548. Li, S.; Hamrick, Y. M.; Van Zee, R. J.; Weltner, W., Jr. *J. Am. Chem. Soc.* **1992**, *114*, 4434−4436.

(29) Prins, R.; Biloen, P.; Van Voorst, J. D. W. *J. Chem. Phys.* **1967**, *46*, 1216−1217. Prins, R.; Van Voorst, J. D. W. *J. Chem. Phys.* **1968**, *49*, 4665−4673.

(30) Ammar, F.; Savéant, J. M. *J. Electroanal. Chem.* **1973**, *47*, 115−125.

(31) (a) Gagné, R. R.; Spiro, C. L. *J. Am. Chem. Soc.* **1980**, *102*, 1443−1444. (b) Goldsby, K. A.; Meyer, T. J. *Inorg. Chem.* **1984**, *23*, 3002−3010. (c) Bligh, R. Q.; Moulton, R.; Bard, A. J.; Piórko, A.; Sutherland, R. G. *Inorg. Chem.* **1989**, *28*, 2652−2658. (d) Richardson, D. E. *Inorg. Chem.* **1990**, *29*, 3213−3217.

(32) No special meaning is attributed to the negative sign of two $\Delta E_{1/2}'(1')$ values. It reflects the scatter of small values which arises probably because minor contributions to $\Delta E_{1/2}$ are neglected.

potential differences of Table 6 can then be formulated as follows:

$$\Delta E_{1/2}'(1) = W_2 + \Delta\Delta G_1 \quad (4)$$

$$\Delta E_{1/2}'(2) = 2W_1 + \Delta\Delta G_2 + E_s \quad (5)$$

$$\Delta E_{1/2}'(1') = W_1 + \Delta\Delta G_1 - E_s \quad (6)$$

$$\Delta E_{1/2}'(2') = W_1 + W_2 + \Delta\Delta G_2 \quad (7)$$

W and $\Delta\Delta G$ may be calculated. However, usually W is underestimated,[33] and the approximation of $\Delta\Delta G$[31d] is less suitable for ions as big as $[MM'M]^{n+}$. These problems can be minimized by considering the ratios W_1/W_2 and $\Delta\Delta G_1/\Delta\Delta G_2$. Insertion of the mean values $\Delta E_{1/2}'(1) = 20$ mV, $\Delta E_{1/2}'(2) = 263$ mV, $\Delta E_{1/2}'(1') = 18$ mV, and $\Delta E_{1/2}'(2') = 59$ mV (from Table 6) as well as $W_1/W_2 = 3.7$[34a] and $\Delta\Delta G_1/\Delta\Delta G_2 = 4/9$[34b] into eqs 4–7 yields $W_1 \approx 140$ mV, $W_2 \approx 40$ mV, the mean values $\Delta\Delta G_1 \approx -30$ mV and $\Delta\Delta G_2 \approx -80$ mV, and $E_s \approx 100$ mV.

These results must be regarded as approximate values for the series $[MM'M]^{n+}$. Since W and $\Delta\Delta G$ are a function of the intermetal distances and the size of the ion, respectively, both are modulated by structural changes. This is particularly true for the change of the metal–Cp distance upon oxidation and for the folding of $[MM'M]^{n+}$ which will depend on M, M', and n. Therefore, the scatter of the $\Delta E_{1/2}$ values in Table 6 is not surprising. Additional data scatter probably arises from the substituent effect E_s. While E_s is additive for many substituted sandwich compounds,[35] silyl groups lead to erratic $E_{1/2}$ values[36] which may even change sign. For the series $[MM'M]^{n+}$ E_s is definitely positive in keeping with the fact that the terminal metallocenes of NiNiNi and FeFeFe are oxidized first.

Spin Transfer between Neighboring Metallocenes of MM'M. As has been demonstrated in ref 9b and the literature cited therein NMR spectroscopy is an efficient tool for studying the spin distribution in sandwich compounds. In the following discussion of the NMR results we will concentrate on MM'M derivatives that contain cobaltocene and nickelocene moieties like FeCoFe, FeNiFe, NiCoNi, and NiNiNi. In these cases, the dipolar contribution to the signal shifts is small[37] and we are dealing with direct π delocalization, i.e., transfer of spin from the metal to the ligand π system without changing the sign.[9b] Occasionally comparison will be drawn to vanadocene- and chromocene-containing molecules. These metallocenes have negative spin density in their ligand π orbitals[9b] which is induced by π polarization. In addition their signal shifts are influenced by delocalization into ligand σ orbitals and dipolar coupling.[9b,27]

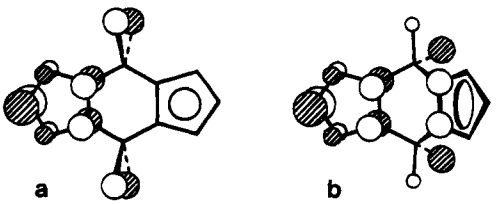

Figure 9. Ligand orbitals reflecting the spin transfer across the Me_2Si groups: (a) flat ligand, (b) bent ligand.

One Paramagnetic Center in FeM'Fe. The signals of all nuclei of the terminal ferrocenes undergo a paramagnetic shift (Table 3) whenever M' has unpaired electrons. This proves that spin is delocalized across the silyl bridges. However, the shifts are much smaller than those found for the nuclei of the central metallocene, and hence the delocalization is not very efficient.

An instructive feature is the signal pattern obtained for the ferrocene moieties. All ^1H and the ^{13}C NMR signals of FeCoFe and of FeNiFe appear at *one* frequency side, and the magnitude of the shifts decreases rapidly on going from C3a/8a to C1/3 and C2. This behavior is expected[38] when the spin is distributed predominantly in the σ system of the ferrocene. The alternative delocalization into the π system of a ferrocene would lead to alternating *low and high* frequency shifts.[39]

A simple MO reasoning illustrates the preference of σ spin. As an example let us take FeCoFe for which we have shown above (discussion related to Figure 6) that the spin is first delocalized from the metal into the e_1-type π_s ligand orbital of the cobaltocene moiety. In Figure 9 the π_s orbital has been combined with the sum of the bonding and antibonding Si–CH_3 orbitals. The result is a variant of the common model of hyperconjugation with little spin density on Si4/8, much on CH_3, and none on C3a/8a (Figure 9a). However, this model has to be modified owing to the folding of the ligand at the Si4–Si8 vector (cf. Figure 4). As can be seen in Figure 9b we now expect selective spin transfer also to C3a/8a. This is confirmed by the NMR signals of C3a/8a which are shifted considerably. Interestingly, the spin densities on C3a/8a and on the equatorial CH_3 carbon atoms C10/12 are rather similar as indicated by the signal shifts of 34.7 and 37.5 ppm, respectively. This is in keeping with the hyperconjugational spin transfer outlined above in that the orientations of C3a/8a and C10/12 relative to the spin-containing ligand π system of the cobaltocene moiety are similar. Thus, the corresponding mean dihedral angles are 61.9° and 58.0° (assuming that FeCoFe and FeVFe have the same structure).

For FeNiFe the same trend is visible in Table 3. Here the shift difference is somewhat larger (C3a/8, 165.7 ppm; C_{eq}, 128.3 ppm) which points to a smaller bending of the bridging ligand. The spin at C3a/8a of FeCoFe and FeNiFe sits in an MO that has a limited admixture of the remaining carbon $2p_z$ AOs of the ferrocene moieties. Hence, further delocalization involves σ-type orbitals.

The NMR signal patterns of the ferrocenes of FeVFe and FeCrFe are less clear-cut owing to competing contributions to the signal shifts. Note, however, that *negative* spin is induced at C3a/8a and the terminal Cps when vanadocene is introduced into MM'M.

What emerges at this point is an experimental model for the effect that one localized unpaired electron in a trimethylenediyl diradical (**G**) has on the second radical center. This information is difficult to obtain from a sterically well-defined radical of

(33) Sutton, J. E.; Sutton, P. M.; Taube, H. *Inorg. Chem.* **1979**, *18*, 1017–1021.

(34) (a) Calculated from eqs 14 and 15 of ref 33 with the metal–metal distances found for FeVFe and the dielectric constant $\epsilon = 27$ for propionitrile. (b) Calculated from eq 11 of ref 31d.

(35) Kuwana, T.; Bublitz, D. E.; Hoh, G. *J. Am. Chem. Soc.* **1960**, *82*, 5811–5817. Perevalova, E. G.; Gubin, E. O.; Smirnova, S. A.; Nesmeyanov, A. N. *Dokl. Acad. Nauk. SSSR* **1964**, *155*, 857–860. Nesmeyanov, A. N.; Denisovitch, L. I.; Gubin, S. P.; Vol'kenau, N. A.; Sirotkina, E. I.; Bolesova, I. N. *J. Organomet. Chem.* **1969**, *20*, 169–176. Yur'eva, L. P.; Peregudova, S. M.; Nekrasov, L. N.; Korotkov, A. P.; Zaitzeva, N. N.; Zakurin, N. N.; Vasilkov, A. Yu. *J. Organomet. Chem.* **1981**, *219*, 43–51. Brunner, H.; Koch, H. *Chem. Ber.* **1982**, *115*, 65–83.

(36) Hoh, G. L. K.; McEwan, W. E.; Kleinberg, J. *J. Am. Chem. Soc.* **1961**, *83*, 3949–3953. Okuda, J.; Albach, R. W.; Herdtweck, E.; Wagner, F. E. *Polyhedron* **1991**, *10*, 1741–1748.

(37) Rettig, M. F.; Drago, R. S. *J. Am. Chem. Soc.* **1969**, *91*, 1361–1370. Köhler, F. H.; Prößdorf, W. *J. Am. Chem. Soc.* **1978**, *100*, 5970–5972.

(38) Köhler, F. H.; Hofmann, P.; Prößdorf, W. *J. Am. Chem. Soc.* **1981**, *103*, 6359–6367.

(39) Köhler, F. H.; Geike, W. A.; Hofmann, P.; Schubert, U.; Stauffert, P. *Chem. Ber.* **1984**, *117*, 904–914.

type **K**. For instance, 9,10-dihydroanthracene$^{\bullet-}$ is not a localized radical,[40] and for 1,4-dihydronaphthalene$^{\bullet-}$ the relevant ^{1}H hyperfine coupling constant could not be determined.[41] Note also that it is still more difficult to obtain ^{13}C EPR data. On the basis of our results we can draw **L** (as derived from FeCoFe and FeNiFe) where the framed part (cf. also **F**) corresponds to **K**. In fragment **N** the relevant ^{13}C NMR results of FeCoFe

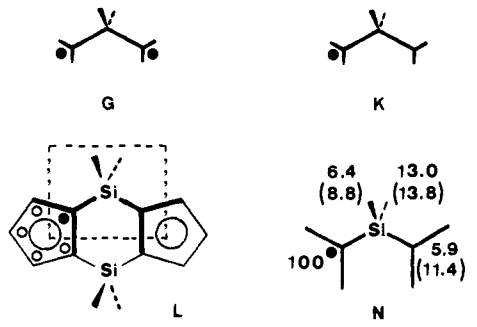

and, in parentheses, FeNiFe are given as an image[42] of the spin distribution. It is gratifying that the numbers, which are normalized to the signal shifts of the "spin source" C4a/7a,[43] are similar, being modulated mainly by geometrical changes (cf. below).

Three Paramagnetic Centers in NiM'Ni. With the results on FeM'Fe in mind one would expect that the NMR data of NiM'Ni are simply the *sum* of those obtained for FeM'Fe and NiFeNi. This seems to be a reasonable approximation for the ^{29}Si NMR signal shift (NiCrNi, 327 ppm, *sum* 308 ppm; NiCoNi, −1107 ppm, *sum* −1067 ppm). However, the agreement is unsatisfactory when the corresponding ^{13}C and (less so) ^{1}H NMR data are compared.

For a key to the understanding of these findings we examine the spin delocalization from a nickelocene to a ferrocene moiety depending on whether it occurs in FeNiFe or NiFeNi. As an image we use again the ^{13}C NMR data, this time those of the common fragment **O**. In **O** the labeled nuclei benefit from

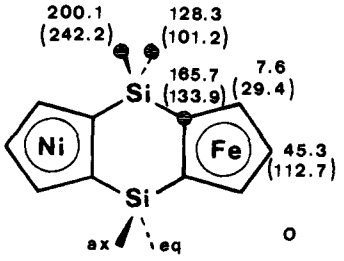

hyperconjugational spin transfer. Their signal shifts sum up to 494.1 and 477.3 (values in parentheses) ppm, respectively, which means that the overall spin transfer deviates by only about 3%.[44] By contrast, the individual shifts are rather different. As derived above (cf. Figure 9b), this must be due to different dihedral angles θ between the relevant Si−C bonds and the nickelocene π system. More explicitly, the bending at the Si−Si vector must be more pronounced in FeNiFe than in NiFeNi. Note that from the NMR data it cannot be concluded whether the bending orients the terminal and central metallocenes *syn* or *anti* relative to each other. Similarly, the data given with **O** illustrate that the remaining signal shifts of the ferrocene depend strongly on the bending of the molecule. Coming back to the ^{29}Si NMR data, it is clear from consulting Figure 9b that the spin density on Si depends much less on the hyperconjugation.[44] Hence, silicon in MM'M (or any NMR-active nucleus in the same position of analogous compounds) is well suited to monitoring interfering spin delocalization.

NMR and the Equilibrium Structure of NiM'Ni. According to the NMR signal shifts of the axial and equatorial CH_3 groups of all the compounds MM'M listed in Tables 3 and 4, a bent equilibrium conformation is adopted in solution. The bending should be influenced not only by changing the metals but also by varying the temperature when it is associated with a soft potential.[45] We have studied this by recording the temperature-dependent ^{1}H NMR spectra of NiVNi. This compound is well suited because for both mononuclear nickelocenes and vanadocenes the NMR signal shifts follow the Curie law closely even if the degeneracy of the singly occupied MOs is lifted by substitution.[46] Hence, the product $\delta^{para}(T/298) = \vartheta$, where ϑ is the reduced paramagnetic signal shift, affords a parallel to the T axis in a ϑ vs T diagram. By contrast, when the bending of NiVNi depends on the temperature, ϑ is not constant any more.

The result is summarized in Figure 10, which shows that, with increasing temperature, the magnitude of $\vartheta(^1H)$ for both the terminal nickelocenes (Cp, H1/3, and H2) and the central vanadocene (H5/7 and H6) decreases. This is easy to understand when we assume that NiVNi flattens upon raising the temperature (due to a strongly unharmonic potential-energy vs bending-angle curve). When NiVNi flattens, less spin is transmitted from the vanadocene to the nickelocenes and vice versa (cf. Figure 9). Since the signs of the spin densities in the ligand π systems of Cp_2V and Cp_2Ni are different, the delocalization across the silyl bridges partly compensates the spin density on each five-membered ring of NiVNi. This effect is reduced with increasing temperature so that the magnitude of the signal shifts increases and eventually approaches the limiting values of flat NiVNi. As can be seen in Figure 10 the accessible temperature window does not allow a completely flat equilibrium structure of NiVNi to be observed.

Correspondingly, the opposite behavior, i.e., a decrease of the magnitude of ϑ with increasing temperature, is observed for NiNiNi (Figure 10). This is expected because the spins on the neighboring Cps have the same sign. For NiNiNi the effect is much smaller than for NiVNi so that it can be observed only for the central nickelocene (H5/7 and H6) which receives spin from two neighbors. We have also investigated the temperature-dependent ^{1}H NMR spectra of NiCrNi, NiCoNi, and CoCrCo. Here both the effect of bending and the thermal population of different orbitals by one unpaired electron lead to a comparable deviation from the Curie law. Hence, both contributions are difficult to separate.

Magnetic Interaction. Effect on the NMR Spectra. In principle the magnetic interaction in di- and oligonuclear compounds shows up in both $\chi_m T$ vs T and ϑ vs T diagrams by a deviation from the Curie law, i.e., from constant $\chi_m T$ and ϑ values, respectively. Unfortunately, the temperature range which is accessible by solution NMR spectroscopy does not allow even qualitative conclusions for the series NiM'Ni to be

(40) Iwaizumi, M.; Bolton, J. R. *J. Magn. Reson.* **1970**, *2*, 278−285.
(41) Joela, H.; Pyykkö, P. *Chem. Phys. Lett.* **1975**, *31*, 574−576.
(42) For a more detailed analysis the spin density on the nuclei next to the observed nucleus must be taken into account; see: Karplus, M.; Fraenkel, G. K. *J. Chem. Phys.* **1961**, *35*, 1312−1323. Yonezawa, T.; Kawamura, T.; Kato, H. *J. Chem. Phys.* **1969**, *50*, 3482−3492.
(43) This signal could not be observed for FeNiFe. For an estimate we use 1450 ppm similar to the values obtained for $(Me_3SiCp)_2Ni$ and NiCrNi in Table 4.
(44) A deviation may originate from different bending of the C−Si bonds out of the nickelocene ligand plane.
(45) Burdett, J. K. In *Accurate Molecular Structures*; Domenicano, A., Hargittai, I., Eds.; Oxford University Press: Oxford, 1992; Chapter 20.
(46) Geike, W. A.; Köhler, F. H. *J. Magn. Reson.* **1983**, *53*, 297−302. Eicher, H.; Köhler, F. H.; Cao, R. *J. Chem. Phys.* **1987**, *86*, 1829−1825.

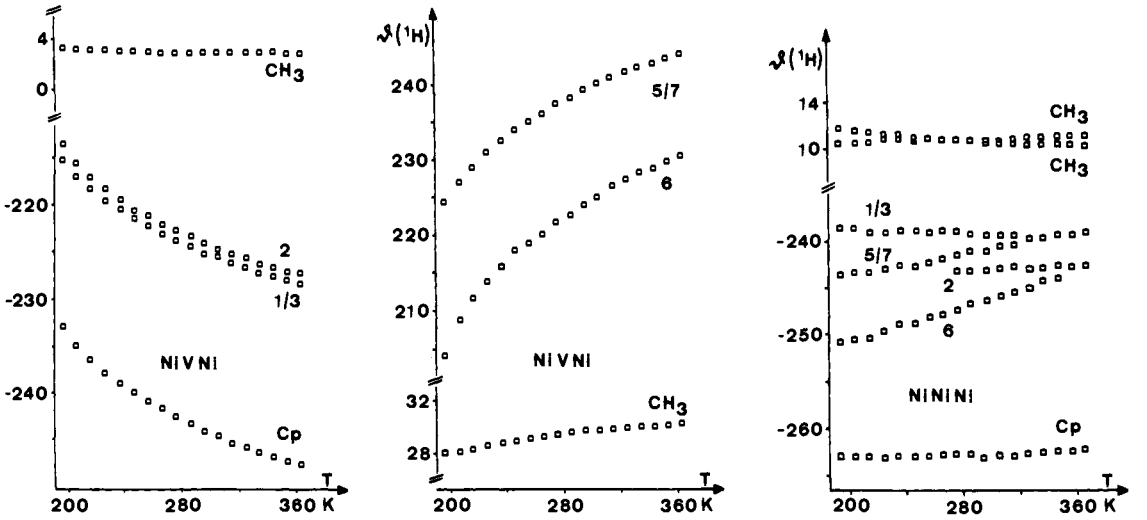

Figure 10. Temperature dependence of the reduced ^{1}H NMR signal shift $\vartheta(^1H) = \delta^{para}(T/298)$ of NiVNi and NiNiNi in parts per million.

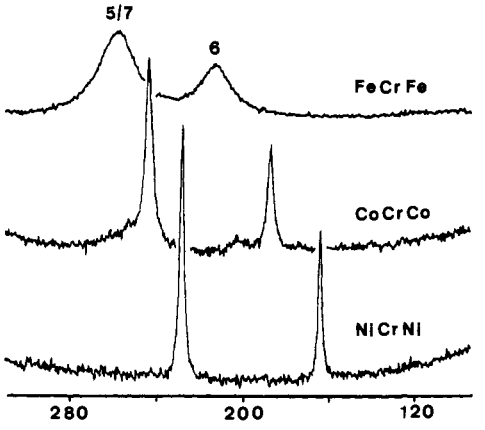

Figure 11. ^{1}H NMR signals of the central chromocene in FeCrFe, CoCrCo, and NiCrNi at 303 K. The scale is in parts per million.

drawn because the exchange parameter is so small ($J < 10$ cm^{-1}). In addition the ϑ vs T curves are perturbed by temperature-dependent changes of the structure and of the population of the orbitals. However, an unambiguous indication of magnetic interaction is given by the half-widths W of the ^{1}H NMR signals (Figure 11).

When passing from FeCrFe to CoCrCo and NiCrNi, the signal half-widths drop from W(H5/7) = 5300 Hz and W(H6) = 4000 Hz to 910 and 740 Hz and to 580 and 450 Hz, respectively. Obviously the transverse nuclear relaxation time $T_{2n} = (\pi W)^{-1}$ is longer when the chromocene is flanked by paramagnetic rather than by diamagnetic metallocenes. This originates from intramolecular exchange narrowing.[47] In a simplified view the magnetic interaction transmits the relaxation at a given metal center to the neighboring one, and in this particular case, W decreases with T_e(M) which is the relaxation time of the unpaired electrons at the metal M. More precisely, in CoCrCo and NiCrNi T_e(Cr) must be influenced by T_e(Co) and T_e(Ni), respectively, and the electrons at Co and Ni must relax faster than at Cr when there is no magnetic exchange. The latter is confirmed by the ^{1}H NMR signal half-widths of the parent metallocenes Cp_2M for which W = 141, 471, and 1231 Hz has been measured at 298 K when M is Co, Ni, and Cr, respectively.[48] Similar values are found for the cobaltocenes in CoCrCo (W(H1/3) = 170 Hz, W(H2) = 190 Hz) and for the nickelocenes in NiCrNi (W(H1/3) = W(H2) = 520 Hz). Note that, owing to magnetic interaction, the proton signals of the chromocene in NiCrNi become about as narrow as those of the nickelocenes whereas for CoCrCo they remain distinctly broader than those of the cobaltocenes. Unfortunately, there does not seem to exist a simple way to obtain the interaction parameter J from NMR line width measurements.

Magnetic Interaction Mechanisms. The quantitative interpretation of the magnetic susceptibility data for NiM′Ni (M = V, Cr, and Ni) leads to local anisotropy parameters D_{Ni} which agree with the values found in nickelocene.[28] The interaction parameter between terminal Ni(II) and central M′ ions is very weak for M′ = V and Cr, and larger for M′ = Ni. This result is in line with the fact that the unpaired electrons of V(II) and Cr(II) occupy e_{2g}-type local orbitals which are essentially localized on the metal atom. On the other hand, the unpaired electrons of Ni(II) occupy e_{1g}*-type local orbitals which have a large contribution of the Cp rings. At the first glance the series NiM′Ni seems to be predestinated for applying the active magnetic orbital approach[49] because two different combinations of next-neighbor magnetic centers are realized in these compounds. Assuming a flat molecule with C_{2h} symmetry for the moment, the magnetic orbitals either have the same symmetry (NiCoNi, NiNiNi) or are orthogonal (NiVNi, NiCrNi, CoCrCo). However, this approach is likely to fail as the ligand orbitals are not far below the metal orbitals. Also the bridging ligands and the magnetic centers are no longer approximately in the same plane as in many coordination compounds.[49] Rather, the bridges are situated below and above the metal−metal vectors. Another unusual feature is the fact that, whatever the symmetry of the magnetic orbitals, the spin is always delocalized predominantly into the ligand π orbitals, albeit with a different sign. This is in contrast with compounds like $CuVO(fsa)_2en{\cdot}CH_3OH$[50] where the spin is delocalized from copper into σ-type ligand orbitals and from vanadium into π-type ligand orbitals.

A more convenient procedure consists in decomposing NiM′Ni into spin-containing ligands and metals as has been outlined in the Introduction. Since the metals are far apart (ca. 6 Å), direct metal−metal interaction can be neglected and we

(47) Bencini, A.; Gatteschi, D. *EPR of Exchange Coupled Systems*; Springer-Verlag: Berlin, 1990; Chapter 6.2, ref 266, Chapter 7.
(48) Hebendanz, N.; Köhler, F. H.; Scherbaum, F.; Schlesinger, B. *Magn. Reson. Chem.* **1989**, *27*, 798−802.
(49) Kahn, O. *Molecular Magnetism*; VCH Publishers: Weinheim, 1993; Chapters 7 and 8.
(50) Kahn, O.; Galy, J.; Journaux, Y.; Morgenstern-Badaraux, L. *J. Am. Chem. Soc.* **1982**, *104*, 2165−2176.

are left with what may be called a *reduced-spin diradical approach* represented by **F′**. Alternatively the central six-membered ring of **F′** could be regarded as a magnetic coupling unit for two spin sources by analogy with the strategy outlined by Dougherty.[11]

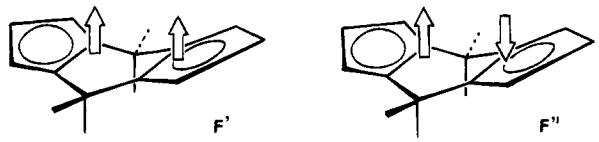

For small cyclic alkanediyls it is known that the triplet state is more stable than the singlet state.[10-12] An important parameter is the angle within the alkanediyl fragment **G**. Thus, when the ring size is increased starting from the butanediyl **H**, the triplet−singlet gap decreases until, eventually, the singlet is more stable in a fragment that is derived from cyclohexane in the chair conformation.[12e] Moreover, a folding of the rings also favors the singlet.[12a,b]

When we extend these findings to the series NiM′Ni, it is clear that the magnetic coupling unit is a cycloalkane-1,3-diene in the boat conformation as visualized in **F′**. It turns out that the magnetic behavior corresponds to a localized diradical with a weak antiferromagnetic interaction.

According to the NMR results obtained for NiNiNi, the spin densities at the alkanediyl positions have the same sign (**F′**). By contrast, the signs are different for NiVNi and NiCrNi so that **F″** is the appropriate model. Nevertheless, the magnetic interaction is antiferromagnetic in all cases. This is understandable because the cycloalkanediyl concept is based on the accidental degeneracy of orbitals. It means that, independent of the sign of the spin densities which are involved, the singlet should always be favored when the degeneracy is lifted for some reason.

Another interesting aspect is that the magnitude of the spin densities can be varied in **F′** or **F″**. Gross changes are accomplished by combining metallocenes with a different number of unpaired electrons while a fine tuning results from the delocalization across the silyl bridges which has been established in the series FeM′Fe. For instance, it can be seen in Figure 11 that the negative spin density on the central chromocene ligand decreases when the positive spin density on the neighboring Cps is increased by changing the terminal ferrocenes ($S = 0$) for cobaltocenes ($S = 1/2$) and nickelocenes ($S = 1$). As expected the reverse effect is deduced from the trend of the nickelocene proton shifts of H1/3, H2, and Cp (Table 4) when passing from NiFeNi to NiCoNi and NiNiNi. This tuning potential should be useful for bridged paramagnetic sandwich compounds in general.

Conclusion

A stepwise approach to doubly Me_2Si-bridged trinuclear metallocenes with the metal sequence MM′M has been realized.

The synthetic steps are based on a mixed-ligand metallocene building block where cyclopentadiene has been fused to the metallocene. The key step is the deprotonation of this building block which may be conducted such that the metallocene remains intact. Further reaction with metal dihalides leads to homo- or heterometallic compounds depending on the metal. This approach is general in two respects: (1) any bridged Cps may be used provided that they can be deprotonated step by step, (ii) extension to well-defined homo- or heterometallic oligomers and polymers is possible.

The compounds MM′M are instructive models for the study of stepwise electrochemical oxidations and (less so) reductions. After sorting out various contributions to the potentials at which the electron transfers occur, the electrostatic interaction between adjacent metallocenes proves to be of similar importance as substituent effects and differential solvation. When every second metallocene is concerned, the electrostatic interaction drops to values close to the limit of resolution of cyclic voltammetry.

The step-by-step principle is also appropriate for describing the structure of MM′M. However, the stepwise stacking of three metallocenes is not ideal because the bridging ligand is bent. Owing to a soft bending potential the temperature dependence of the bending is visible in the NMR spectra.

The bending of MM′M is crucial for the delocalization of the spin density from one metallocene to the next. By fusing para- and diamagnetic metallocenes in the series FeM′Fe, it was established that the delocalization to a neighboring metallocene is mainly due to hyperconjugation which is mediated by the bridging Me_2Si groups. When passing to compounds which consist of three paramagnetic centers as in NiM′Ni, the intermetallocene delocalization leads to changes of the overall spin density on each Cp ligand. These changes may be exploited for adjusting the spin density systematically. It should be noted that the procedure is applicable to any paramagnetic multimetal compounds which yield NMR spectra.

The molecules studied so far by magnetic measurements (NiVNi, NiCrNi, NiNiNi) show antiferromagnetic interaction regardless of whether the signs of the spin density on adjacent Cps are alike or unlike. This behavior can be understood by regarding the bridging ligand as a localized diradical of the cycloalkanediyl type where the radical sites have a reduced spin density. In the present cases the "diradical" is part of a six-membered ring for which the interactions known from genuine cycloalkanediyls[11] lead to a low-spin ground state.

What emerges from this analogy is the potential use of bridged paramagnetic π complexes as models for organic diradicals and polyradicals. For instance, the spin delocalization could be investigated conveniently. Advantages are the thermal stability of the π complexes and the versatility of the NMR method.

Experimental Section

All reactions and the characterization of the new compounds were carried out under exclusion of air and moisture. This was achieved by applying a combination of Schlenk and cannula techniques. Argon was used as the inert gas, the glassware was flame-dried in vacuo, and the solvents were purified conventionally. The elemental analyses were performed by the Inorganic Microanalytical Laboratory at Garching.

Bis(cyclopentadienyliron)−bis-(μ-1,2,3,3a,8a-η⁵-3a,4,7a,8-tetrahydro-4,4,8,8-tetramethyl-4,8-disila-*s*-indacene-3a,7a-diyl)metal Compounds FeM′Fe. Solutions of **5** were prepared starting from 1.8 g (7 mmol) of **1a** and **1b** as described previously.[16] The reaction with the metal halides gave the following results.

FeVFe. A 1.3 g (3.5 mmol) amount of $VCl_3(THF)_3$ was dissolved in THF, and 0.7 g (10.7 mmol) of zinc dust was added. After stirring for 48 h at room temperature, a light-green solid and a green solution were obtained. When the solution of **5** in THF was added to the suspension via cannula, the mixture darkened. It was stirred for 2 h; subsequently the solvent was removed under reduced pressure, and the remainder was extracted with three portions of 200 mL of hexane. Concentrating the solution and slow cooling gave a powder, which, after recrystallization from toluene, gave 0.65 g (24% relative to **1a**/**1b**) of FeVFe as ocher-yellow microcrystals melting at 145 °C under decomposition. MS (*m*/*z* (%)): 777 (100), M^+; 413 (8), $CpFeLV^+$; 389 (28), M^{2+}; 364 (4), $CpFeL^+$; 293 (9); 277 (4); 243 (5); 121 (2), $CpFe^+$ (L = bridging ligand $C_{14}H_{18}Si_2$). Anal. Calcd. for $C_{38}H_{46}Fe_2Si_4V$: C, 58.68; H, 5.96; Fe, 14.36. Found: C, 58.49; H, 5.75; Fe, 14.40.

FeCoFe. A 0.45 g (3.5 mmol) amount of anhydrous $CoCl_2$ was dissolved in a mixture of 50 mL of Et_3N and 150 mL of THF. The blue solution was added to the solution of **5** in THF whereupon the color darkened. Workup as described for FeVFe yielded 1.13 g (41% relative to **1a/1b**) of orange-brown microcrystals of FeCoFe. Mp: 160 °C dec. MS (*m/z* (%)): 785 (100), M^+, 393 (26), M^{2+}; 301 (4); 121 (3), $CpFe^+$. Anal. Calcd. for $C_{38}H_{46}CoFe_2Si_4$: C, 58.09; H, 5.90. Found: C, 58.34; H, 5.92.

FeNiFe. A 0.70 g (2.15 mmol) amount of $NiBr_2(THF)_{1.5}$ was added to a solution of **5** (prepared from 1.46 g (4.0 mmol) of **3**) in 100 mL of THF and 1.9 mL of a 2.2 M solution of MeLi in ether. The green mixture was worked up similarly as described above. Recrystallization from acetone yielded 0.77 g (49% relative to **3**) of yellow-green microcrystals of FeNiFe which decomposed above 180 °C. MS (*m/z* (%)): 784 (100), M^+; 421 (8), $CpFeLNi^+$; 392 (26), M^{2+}. Anal. Calcd. for $C_{38}H_{46}Fe_2NiSi_4$: C, 58.10; H, 5.90; Fe, 14.22; Ni, 7.47; Si, 14.30. Found: C, 57.64; H, 5.74; Fe, 13.91; Ni, 7.42; Si, 14.8.

Bis(cyclopentadienylnickel)−bis-(μ-1,2,3,3a,8a-η⁵-3a,4,7a,8-tetrahydro-4,4,8,8-tetramethyl-4,8-disila-*s*-indacene-3a,7a-diyl)metal Compounds NiM'Ni (M' = V, Cr, Co, Ni). The series of compounds was prepared without isolating **4a/b**. Thus, for each experiment 4.55 g (18.6 mmol) of **1a/b** in 200 mL of THF was cooled to −78 °C and treated with 11 mL of a 1.7 M solution of nBuLi in hexane. After the solution had been brought to room temperature 46 mL of a 2.02 M solution of CpNa in THF and 20 g (61 mmol) of $NiBr_2(THF)_{1.5}$ were added under stirring. The green mixture was stirred for 1 h, the solvents were stripped, and the remainder which contained **4a/b** and Cp_2Ni was extracted with three 100 mL portions of hexane. A suspension of lithium piperidide was prepared at room temperature from 1.5 mL (15 mmol) of piperidine and 3.8 mL of a 1.7 M solution of nBuLi in hexane, and cooled to −78 °C. The suspension was quickly transferred via cannula to the hexane solution of the nickelocenes which were also kept at −78 °C. After stirring overnight at −78 °C, the gritty solid had become flocculent. The mixture was brought to 25 °C within 12 h, the green solid was allowed to settle, and the green solution was removed via cannula. The solid was washed with hexane until the solution was colorless (four times) and dissolved in 300 mL of THF. The ^{13}C and ^{29}Si NMR spectra which were run with a concentrated sample were consistent with the formation of **6**.[17]

NiVNi. A 2.70 g (7.2 mmol) amount of $VCl_3(THF)_3$ in THF was reduced with zinc dust as described for FeVFe. When the resulting mixture was combined with the solution of **6** in THF, the color became dark green. After stirring for 1 h and stripping the solvents, the solid residue was extracted four times with 250 mL of hexane. Since the ^1H NMR spectra showed that the byproducts decreased from one extraction to the next, the last fractions were combined and slowly concentrated until a light green powder precipitated. Recrystallizing from toluene gave small green crystals which transformed into a powder on drying in vacuo. Yield: 0.95 g (17% relative to $VCl_3(THF)_3$). Mp: 230 °C dec. MS (*m/z* (%)): 781 (3), M^+; 660 (2), M^+-CpNi+2; 593 (2), M^+-Cp_2Ni; 481 (7), $CpNiLVCp^+$; 366 (16), $CpNiL^+$+1; 293 (14), VL^+; 188 (100), Cp_2Ni^+; 123 (85), $CpNi^+$. Anal. Calcd. for $C_{38}H_{46}Ni_2Si_4V$: C, 58.25; H, 5.92; Ni, 14.99; Si, 14.34. Found: C, 57.14; H, 5.93; Ni, 14.70; Si, 14.7.

NiCrNi. Similarly the addition of 1.60 g (8.0 mmol) of $CrCl_2(THF)$ to the solution of **6** in THF and workup including crystallization from toluene gave mossy green crystals which were shown to be the toluene solvate NiCrNi(toluene) by elemental analysis. Under reduced pressure the crystals lost toluene and disintegrated. Crystallization from hexane yielded 2.3 g (37% relative to $CrCl_2(THF)$ of olive-green platelets. Mp: 230−240 °C dec. MS (*m/z* (%)): 782 (94), M^+; 660 (7), M^+-CpNi+1; 482 (8); 483 (4); 484 (5); 485 (2); 488 (13); 489 (5); 490 (12); 491 (4); 493 (5); 366 (8), $CpNiL^+$; 188 (28), Cp_2Ni. Anal. Calcd. for $C_{45}H_{54}CrNi_2Si_4$: C, 61.65; H, 6.21; Ni, 13.39; Cr, 5.93. Found: C, 61.14; H, 6.35; Ni, 13.78; Cr, 5.71.

NiCoNi. A solution of 0.90 g (7.0 mmol) of anhydrous $CoCl_2$ in a mixture of 70 mL of Et_3N and 200 mL of THF was poured into the solution of **6** in THF. After workup and crystallizing from toluene 1.9 g (34% relative to **1a/b**) of NiCoNi was obtained as green platelets. Mp: 150 °C dec. MS (*m/z* (%)): 789 (89), M^+; 668 (33), M^+-$CpNiL^+$+2; 601 (15), M^+-Cp_2Ni; 396 (17), M^{2+}; 366 (8), $CpNiL^+$; 188 (68), Cp_2Ni; 123 (52), $CpNi^+$. Anal. Calcd. for $C_{38}H_{46}CoNi_2Si_4$: C, 57.67; H, 5.86; Ni, 14.83; Co, 7.44. Found: C, 57.31; H, 5.67; Ni, 14.98; Co, 7.10.

NiNiNi. A 2.61 g (8.0 mmol) amount of $NiBr_2(THF)_{1.5}$ was added to the solution of **6** in THF. Workup and crystallizing from toluene gave NiNiNi as a yellow-green powder. Yield: 3.24 g (51% relative to $NiBr_2(THF)_{1.5}$). MS (*m/z* (%)): 790 (100), M^+ 725 (2), M^+-Cp; 423 (36), $CpNiLNi^+$; 395 (24), M^{2+}; 123 (16), $CpNi^+$. Anal. Calcd. for $C_{38}H_{46}Ni_3Si_4$: C, 57.68; H, 5.86; Ni, 22.26. Found: C, 57.73; H, 5.89; Ni, 21.40.

Bis(cyclopentadienylnickel)−bis-(μ-1,2,3,3a,8a-η⁵-3a,4,7a,8-tetrahydro-4,4,8,8-tetramethyl-4,8-disila-*s*-indacene-3a,7a-diyl)iron NiFeNi. From 1.16 g (2.14 mmol) of **7a** and **7b** dissolved in 150 mL of THF and 3 mL of a 1.45 M solution of nBuLi in THF the dianion **8** was prepared as described previously.[16] To the orange solution were added 15 mL of a 1.43 M solution of CpNa in THF and, after heating to 60 °C, 4.2 g (12.9 mmol) of $NiBr_2(THF)_{1.5}$. The resulting green suspension was stirred for 1 h, the solvent was removed under reduced pressure, and the mustard-colored residue was extracted three times with 80 mL of toluene heated to 70 °C. After stripping the solvent from the green extract, the solid product was subjected to sublimation (1 Pa, 40−60 °C bath temperature) in order to remove Cp_2Ni. The remainder was dissolved in a minimum of toluene and filtered through silica (Merck 60, 63−200 μm, 5 cm layer in a frit) whereupon the upper part of the silica became brown and a green solution was obtained. From the solution the toluene was stripped, the solid was dissolved in 100 mL of boiling acetone, and the mixture was cooled to −20 °C for 12 h. The resulting precipitate was filtered and recrystallized (−40 °C) from a minimum of THF (saturated solution at 45 °C) to yield 1.05 g (62% relative to **7a/b**) of NiFeNi as olive-green microcrystals. The compound decomposed without melting when heated above 200 °C. MS (*m/z* (%)): 786 (100), M^+; 393 (24), M^{2+}; 123 (18), $CpNi^+$. Anal. Calcd. for $C_{38}H_{46}FeNi_2Si_4$: C, 57.89; H, 5.88; Ni, 14.89. Found: C, 57.76; H, 6.03; Ni, 13.88.

Bis(cyclopentadienylcobalt)−bis-(μ-1,2,3,3a,8a-η⁵-3a,4,7a,8-tetrahydro-4,4,8,8-tetramethyl-4,8-disila-*s*-indacene-3a,7a-diyl)chromium CoCrCo. A solution of 5.30 g (40.8 mmol) of anhydrous $CoCl_2$ in 100 mL of Et_3N and 300 mL of THF was poured at room temperature under stirring into a solution of **2** in THF prepared from 3.33 g (13.7 mmol) of **1a/b** and 1.7 mL of a 1.7 M solution of nBuLi in hexane as described for NiM'Ni. The resulting brown mixture was freed from the solvents, and the solid was extracted with 400 mL of hexane. After cooling the solution to −78 °C, a suspension of lithium piperidide (from 1 mL (10.1 mmol) of piperidine and 5.6 mL of a 1.7 M solution of nBuLi in hexane which was also kept at −78 °C) was added via cannula. The mixture was stirred overnight and then brought to ambient temperature within 12 h. The brown cloudy precipitate which had formed was allowed to settle, the brown solution was removed, and the solid was washed four times with 300 mL of hexane. When the solid was dissolved in 300 mL of THF and 1.0 g (5.0 mmol) of $CrCl_2$-(THF) was added, the color changed from brown to green. After stirring the mixture for 1 h, the solvents were stripped, the residue was extracted with three 250 mL portions of hexane, and the combined fractions were reduced to one-third. From this solution a green precipitate formed after standing for several hours. It was recrystallized twice from toluene and gave 0.4 g of green microcrystals of CoCrCo. Yield: 10% relative to $CrCl_2(THF)$. Mp: 160−170 °C dec. MS (*m/z* (%)): 784 (59), M^+; 661 (3), M^+ − CpCo; 545 (16); 367 (100), $CpCoL^+$; 189 (14), Cp_2Co; 124 (6), $CpCo^+$. Anal. Calcd. for $C_{38}H_{46}Co_2CrSi_4$: C, 58.14; H, 5.91. Found: C, 58.24; H, 6.06.

Spectra. The mass spectra were obtained from a Varian MAT 311A and a Finnigan MAT 90 spectrometer under electron impact (70 eV) conditions. The most abundant isotopes were used for calculating the reported ions, and only one (rounded) mass is given for M^{2+}. The NMR spectra were recorded with a Bruker CXP 200, a Bruker MSL 300, and a Jeol JNM GX 270 spectrometer. Tubes equipped with ground glass fittings and stoppers were used, and the signals were measured relative to the solvent peaks. Calculation relative to the corresponding signal shifts of isostructural diamagnetic iron derivatives[19] by using known solvent signal shifts[51] gave the paramagnetic shifts. In

(51) Kalinowski, H.-O.; Berger, S.; Braun, S. *^{13}C-NMR-Spektroskopie*; Georg Thieme Verlag: Stuttgart, 1984; p 74.

a few cases the signals of similar nuclei (e.g., H2 and H6) could not be distinguished in FeFeFe. Then a mean shift was used as the reference. If not stated otherwise, the spectra were measured at 293 or 305 K. The shifts were calculated to the standard temperature 298 K by assuming that, in the narrow temperature range, the deviation of the Curie law was small. When temperature-dependent spectra were available, the shifts were interpolated for 298 K.

Cyclovoltammetry. The equipment used has been described previously.[16,19] Solutions in purified propionitrile which were 0.10–0.13 M in the supporting electrolyte nBu_4NPF_6 and $(1-5) \times 10^{-4}$ M in the compound were studied at ambient temperature and near −20 °C. For referencing internal Cp_2Co^+, Cp_2Fe (1345 mV relative to Cp_2Co/Cp_2Co^+ at −20 °C) was used.

Magnetic Measurements. These were carried out with two apparatus, namely, a Faraday-type magnetometer equipped with a He continuous-flow cryostat working in the 4.2–300 K temperature range, and a SQUID magnetometer working down to 1.7 K. The data were corrected of the diamagnetism of the core estimated from Pascal's tables.

Crystal Structure Analysis. A crystal of 0.01 mm^3 was sealed under argon into a glass capillary, and the measurements were carried out at −50 °C. Diffractometer measurements yielded a triclinic cell (a = 10.075(2) Å, b = 10.268(1) Å, c = 9.019(1) Å, α = 96.93(1)°, β = 95.78(1)°, γ = 95.15(1)°) and the space group $P\bar{1}$.

The structure was solved by Patterson methods (SHELXS-86). The anisotropic refinement of the non-hydrogen atoms was done by using the program SHELXL-93, by including all structure factors with $F_o \leq 4.0\sigma(F_o)$, and by refining the Cp rings as regular pentagons. Idealized angles were used for the refinement of the hydrogen atoms of Cp ($U_{iso} = 1.2U_{eq}$ of the carbon atom), and the hydrogen atoms of the CH_3 groups were calculated in idealized geometry (C–H 0.96 Å, $U_{iso} = 1.5U_{eq}$ of the carbon atom) and rotated to positions of maximum electron density. The refinement was terminated with R = 0.029; a difference synthesis was featureless. Further details are given in the supplementary material.

Acknowledgment. We thank J. Riede for his help in the X-ray analysis and Dr. J. Blümel for assistance in the NMR spectroscopy. We also acknowledge support from the European Union program Human Capital and Mobility (Magnetic Molecular Materials Network), the Deutsche Forschungsgemeinschaft, the Fonds der Chemischen Industrie, and Wacker Chemie GmbH.

Supplementary Material Available: Crystallographic data, fractional atomic coordinates, equivalent isotropic displacement parameters, and anisotropic displacement parameters (Tables VII–IX) (3 pages); observed and calculated structure factors for FeVFe (Table X) (7 pages). This material is contained in many libraries on microfiche, immediately follows this article in the microfilm version of the journal, and can be ordered from the ACS; see any current masthead page for ordering information.

JA9425905